# Structure-based optimization of a PDZ binding motif within a viral peptide stimulates neurite outgrowth

Zakir Khan, Elouan Terrien, Florent Delhommel, Cynthia Lefebvre-Omar, Delphine Bohl, Sandrine Vitry, Clara Bernard, Juan Morua Ramirez, Alain Chaffotte, Kevin Ricquier, et al.

# Structure-based optimization of a PDZ-binding motif within a viral peptide stimulates neurite outgrowth

**Zakir Khan[1]*†, Elouan Terrien[2]*, Florent Delhommel[2], Cynthia Lefebvre-Omar[3], Delphine Bohl[3], Sandrine Vitry[1], Clara Bernard[1], Juan Ramirez[2], Alain Chaffotte[2], Kevin Ricquier[2], Renaud Vincentelli[4], Henri Buc[5], Christophe Prehaud[1**], Nicolas Wolff[2**$], and Monique Lafon[1***].**

From the [1]Institut Pasteur, Unité de Neuroimmunologie Virale, UMR 3569, CNRS, Paris, (75015) France; [2]Institut Pasteur, Unité de RMN des Biomolécules UMR 3528, CNRS, Paris, (75015) France; [3]Institut du Cerveau et de la Moelle épinière, ICM, U1127 INSERM, UMR 7225 CNRS, Sorbonne Université, Paris, (75013) France; [4]Unité Mixte de Recherche 7257, CNRS Aix-Marseille Université, Architecture et Fonction des Macromolécules Biologiques (AFMB), Marseille (13009) France; [5]Institut Pasteur, Paris (75015) France

Running title: *Interfering peptides stimulating neurite outgrowth*

† Present address: Department of Biomedical Sciences, Cedars-Sinai Medical Center, 8700 Beverly Blvd., Los Angeles, CA 90048, USA.

$ Present address: Institut Pasteur Unité Récepteurs-Canaux, UMR 3571, CNRS, Paris (75015) France

*These authors contributed equally, as joint first authors

** These authors contributed equally as lead authors

*** To whom correspondence should be addressed: Monique Lafon, Institut Pasteur, 25 rue du Dr Roux 75724 Paris Cedex 15, monique.lafon@pasteur.fr . Tel+33145688752

**Key words:** structure-function analysis, interfering peptide, microtubule-associated Ser/Thre kinase 2 (MAST2), PDZ domain, neuritogenesis, neurodegeneration, kinase inhibition, RABV G-protein

---

## Abstract

Protection of neuronal homeostasis is a major goal in the management of neurodegenerative diseases. Microtubule-associated Ser/Thre kinase 2 (MAST2), inhibits neurite outgrowth, and its inhibition therefore represents a potential therapeutic strategy. We previously reported that a viral protein (G-protein from rabies virus) capable of interfering with protein–protein interactions between the PDZ domain of MAST2 and the C-terminal moieties of its cellular partners counteracts MAST2-mediated suppression of neurite outgrowth. Here, we designed peptides derived from the native viral protein to increase the affinity of these peptides for the MAST2 PDZ domain. Our strategy involved modifying the length and flexibility of the non-interacting sequence linking the two subsites anchoring the peptide to the PDZ domain. Three peptides, Neurovita1 (NV1), NV2, and NV3, were selected, and we found that they all had increased affinities for the MAST2 PDZ domain, with $K_d$ values decreasing from 1300 to 60 nM, while target selectivity was maintained. A parallel biological assay evaluating neurite extension and branching in cell cultures revealed that the NV peptides gradually improved neural activity, with the efficacies of these peptides for stimulating neurite outgrowth mirroring their affinities for MAST2-PDZ. We also show that NVs can be delivered into the cytoplasm of neurons as a gene or peptide. In summary, our findings indicate that virus-derived peptides

targeted to MAST2-PDZ stimulate neurite outgrowth in several neuron types, opening up promising avenues for potentially using NVs in the management of neurodegenerative diseases.

## Introduction

The stabilization of homeostasis and the promotion of neuron survival are major challenges in the treatment of neurodegenerative diseases and neuron protection after nerve damage. The PI3K/AKT signaling pathway mediates cell survival and promotes resistance to apoptosis by inactivating components of the apoptotic machinery (1,2). The PI3K/AKT signaling pathway also controls neuronal morphology and the dynamic formation of neurites during development. In mature neurons, the PI3K/AKT signaling pathway activates neurite extension and branching (referred to hereafter as neurite outgrowth).

Neurite outgrowth is strongly repressed by inhibitory factors, such as PTEN (phosphatase and tensin homolog deleted on chromosome ten), an upstream inhibitor of the PI3K/AKT/mTOR cascade-signaling pathway (3-5). *PTEN* silencing restores neurite outgrowth in various types of neurons (6-9) and promotes branching (8,10,11) in cells and *in vivo*. Neurite outgrowth in human neuroblastoma cells (SHSY5Y) could be restored by the silencing of an AGC kinase widely expressed in the nervous system, the microtubule-associated serine-threonine kinase 2 (MAST2) (12). The similar impacts of gene silencing observed for both PTEN and MAST2 probably reflects the occurrence of protein-protein interactions between these proteins, involving the PDZ domain (post-synaptic density protein 95, *Drosophila* disc large tumor suppressor and Zona occludens 1) of MAST2. Valiente and coworkers (13) showed that the PDZ domain of MAST2 (MAST2-PDZ) binds the C-terminal PDZ-binding motif (PBM) of PTEN, greatly increasing the phosphorylation of PTEN by MAST2 at sites thought to control both the cellular distribution and activity of PTEN. Through the formation of this binary complex, MAST2 and PTEN act in synergy to inhibit the signal transduction pathways required for neuronal survival, neurite outgrowth and regeneration (13-15). Specific disruption of the complex formed by MAST2-PDZ and the PBM of PTEN would therefore be expected to block this inhibition, stimulating neuron survival, neurite outgrowth and regeneration.

We previously showed that virulent strains of the rabies virus (RABV) promote the survival of infected neurons, through the binding of the C-terminus of the viral G protein to MAST2 *via* a PDZ/PBM interaction resembling that between PTEN and kinase (16). We have shown that the RABV G-protein of virulent strains promotes neurite outgrowth by activating the AKT signaling pathway in a PBM-dependent manner (16,17). Using NMR, we determined the high-resolution structures of the PDZ/PBM complexes formed by MAST2 and PTEN, and by MAST2 and RABV G-protein (18,19). The PBMs of RABV G-protein and PTEN both display an unconventional mode of binding to MAST2-PDZ involving two anchor sites and similar binding affinities enabling these proteins to compete at the binding site of MAST2-PDZ. Finally, we have shown that the expression of RABV G-protein in human neuroblastoma cells modifies the cellular distribution of PTEN in a PBM-dependent manner (18,19). Thus, the C-terminal sequence of RABV G-protein promotes neuron survival by disrupting the complex formed between MAST2-PDZ and PTEN. MAST2-PDZ appears to be a promising target for neuroprotective therapy. We aimed to design short interfering polypeptides capable of efficiently promoting neurite outgrowth by targeting MAST2-PDZ.

In this article, we first identified the minimal core of the viral G-protein required for a peptide to trigger neurite outgrowth in different types of neurons after lentiviral vector-mediated transduction. Then, using the original PBM of the RABV G-protein (NV1-PBM) as our starting material, we performed a rational search for sequence modifications increasing the affinity of the PBM for MAST2-PDZ. We investigated the efficacy of three peptides — Neurovita1 (NV1), Neurovita2 (NV2) and Neurovita3 (NV3)—by comparing their capacities to trigger neurite extension and branching in neurons transduced with the corresponding lentiviral vectors. The affinity and specificity profiles of the NV-PBMs were checked with a collection of 222 human PDZ

domains (20). Finally, NV3-PBM was delivered to cells as a peptide after fusion to a cell-penetrating molecule (CPM), as an alternative to lentivectors transduction with the aim to use it as a potential drug compound for neurodegenerative diseases, and the capacity of the peptide to stimulate neurite outgrowth was assessed.

## Results

### *Relevance of the in vitro biological models we chose to study Neurovita properties*

The aim of the study is to analyze the biological properties of different sequences of Neurovita based on the basis of the strength of their interaction with the PDZ of MAST2. Thus, it is required that the selected cell models used in the biological assays do express MAST2. MAST2 expression was detected by Q-PCR in human neuroblastoma, mouse primary cells and rat neuroscreen (NS) cells, (Fig S1A) and by immunocytochemistry using a specific MAST2 antibody in human neuroblastoma and rat NS (Fig S1B). In addition, we confirmed that *MAST2* silencing in the human SH-SY5Y neuroblastoma cell line used in our laboratory stimulates neurite outgrowth (Fig 1A) as previously shown by Loh S et al (12).

### *Construction of the initial Neurovita 1 (NV1) peptide*

The infection of neurons with RABV leads to the expression of five viral proteins, the N, M, G, NS and L proteins. The G-protein, (Fig. 1B Diagram of the full-length RABV G-protein) is a 524 aa type I glycoprotein. It is synthesized in the endoplasmic reticulum (ER) of the soma, and is then glycosylated in the Golgi apparatus (see G protein trafficking in Fig.1B). The G-protein then migrates to the plasma membrane of the neurites, where it associates with the viral RNP and M protein, for virion formation and egress by budding. The G-protein is attached to ER─and plasma membranes *via* its unique transmembrane domain (TM). The ectodomain (EC) of the G-protein is located within the luminal compartment of the ER initially, and then at the cell surface after fusion to the plasma membrane. During G-protein trafficking from the ER to the plasma membrane, the cytoplasmic domain (Cyto) containing the C-terminal PBM is always exposed to the cytoplasm of the somato-dentritic neuronal area, where it can interact with cellular partners such as MAST2, *via* its PDZ domain. The formation of this complex triggers neurosurvival signaling pathways and the localization of MAST2 to a submembrane area of the infected cells (16).

We identified the parts of the viral G-protein required for a short interfering polypeptide to mimic the neurosurvival properties of the viral G-protein. We constructed a mini-RABV G-protein, NV1, (Fig. 1B, NV1 scheme). NV1 harbours a 99.6% deletion of the EC domain but retains the SP, TM and Cyto-PBM domains, which are required for its processing. We investigated the role of the C-terminal PBM in the biological properties of NV1 by generating a polypeptide lacking four aa at the C-terminus, NV1delta (NV1Δ) (Fig.1B NV1Δ scheme). The properties of the NVs were investigated following the transduction of two types of neuronal cell lines: SH-SY5Y cells and NS. The NV1 and NV1Δ proteins were detected by western blotting (WB) with a specific Cyto-G antibody in SHSY5Y cell lysates 24 h after transduction (Fig. 1C) and in NS cell lysates 48 h after transduction (Fig.1D). Neurite outgrowth in NV1Δ-transduced cells was similar to that in non-transduced cells (Fig. 1 C and D). By contrast, NV1 triggered a significant stronger neurite outgrowth by comparison to NV1Δ in both types of cell [1.6 times stronger in SHSY5Y cells 30 h after transduction, and 3.1 times stronger in NS cells 72 h after transduction (Fig. 1C and D, right panels and Fig S2 for NeuronJ drawings].

Neurite outgrowth was also triggered in neurons other than neuroblastoma and pheochromocytoma cells grown in the presence of a DF medium (NGF or db-cAMP for NS and SHSY5Y, respectively). The effects of NV1 were assessed in transduced human IPSc derived motor neurons (Fig. 2A), and in transduced E16 mouse primary cortical neurons (Fig. 2B). In these two models, where lentivirus transduced more than 80% of cells (data not shown), NV1 stimulated neurite outgrowth more efficiently than NV1Δ (1.8-fold increase in human motor neurons and 1.2-fold increase in primary mouse cortical neurons). Thus, NV1 induces neurite outgrowth in a PBM-dependent manner in primary cultures of neurons, whether of mouse and human origin.

These results show that it is feasible to construct a polypeptide conserving the properties of the

viral G protein if this polypeptide includes the cytoplasmic part of the G protein and the last 4 aa from the C-terminus of the PBM.

***Optimization of NV-PBMs sequences to improve their binding to MAST2-PDZ***

We previously solved the high-resolution structures of the C-terminal sequences of 13 residues of PTEN and RABV G-protein bound to MAST2-PDZ and calculated their affinities (1.99 and 1.26 µM, respectively) (19). We discovered that, unlike most PBMs, the PBMs of PTEN and of viral G protein have an unusually large interaction surface (700Å$^2$), encompassing not only the 4 aa at the C-terminus of the PBM (-QTRL$_{COOH}$ for G protein and -ITKV$_{COOH}$ for PTEN), but also a second anchoring region located at the N-terminus of the assayed peptides, ($_{NH2}$SW- for G protein and $_{NH2}$PF- for PTEN), (Fig. 3A). The sequences interacting with MAST2-PDZ are $_{NH2}$SWESHKSGGQTRL$_{COOH}$ and $_{NH2}$PFDEDQHTQITKV$_{COOH}$ for G protein and PTEN, respectively. They contain three contiguous regions, the N-terminal anchor (2 aa residues in blue in Fig. 3), a linker (7 aa residues in green) and the conventional C-terminal anchor (4 aa residues in orange).

We began our search for peptides with a greater affinity for MAST2-PDZ by focusing on the 13 residues at the C-terminal end of the viral G protein ($_{SW}$Cyto 13$_{QTRL}$) and human PTEN ($_{PF}$PTEN$_{ITKW}$). Using our high-resolution NMR structures of MAST2-PDZ/peptide complexes, we rationally designed sequences likely to increase the enthalpic contribution and decrease the entropic cost of binding to MAST2-PDZ. Isothermal titration calorimetry was performed in binding experiments with the MAST2-PDZ domain; the thermodynamic quantities associated with peptide binding were compared with the data obtained for the original sequences (18,19).

We focused on optimizing the seven-residue linker (positions -4 to -11) tethering the N-terminal and C-terminal anchors of viral G-protein onto MAST2-PDZ, which has been shown to be a sensitive target for improving binding affinity(18) (21). By contrast, we kept the C-terminal anchor -QTRL$_{COOH}$, which maintains specificity, intact, together with the N-terminal dipeptide $_{NH2}$SW-, which significantly increases binding affinity.

We began by maintaining linker length at seven residues and mutating exposed residues to increase the degree of hydrophobic contact of the two original linker sequences [S(-6) and K(-7) for $_{SW}$ Cyto13$_{QTRL}$ or D(-8), and D(-10) for $_{PF}$PTEN$_{ITKV}$] (Fig. 3B).

These modifications increased affinity modestly with respect to $_{SW}$Cyto13$_{QTRL}$, by a factor of three at best (Fig. 3B). This was not unexpected, because, for all assayed sequences with a linker of this length, any decrease in the free enthalpy of binding is strongly compensated by a simultaneous decrease in the associated entropy. The mean compensation between these two thermodynamic quantities was estimated at 80% from the slope of the plot of the corresponding data displayed in Fig. 3C. By analyzing the kinetic behavior of potential candidates with seven-residue linkers, we previously showed (18) that the flexibility of linker sequences strongly affects their affinity for MAST2-PDZ. However, the high-resolution 3D structures of the PDZ/PBM complexes provided no evidence of contact between MAST2-PDZ and the linker present in the Cyto13 of viral G protein or PTEN. This discrepancy was probably mostly due to the conformational entropy of the potential ligand in the unbound state, because the polypeptides most disordered when free in solution were the poorer binders. We therefore reduced linker length from 7 to 5 aa and designed seven new sequences, for which we compared binding abilities (lines 5 to 11 in Fig. 3B). The deletion of 2 aa from sequence 442 to generate sequence 441 led to a significant increase in the entropy of binding with no marked change in enthalpy contribution, resulting in a four-fold increase in affinity. For these shorter sequences, the compensation between the enthalpy and the entropy terms remained at 80% (Fig. 3C). The binding affinities of the new candidates were also modulated by the substitution of one or both of the doublet glycine present at positions -4 and -5. The G to Q change at position -4 yielded the candidate with the highest affinity, PBM 454.

We retained the two sequences with the highest affinities from this second step in peptide design: PBM 441 (which we named NV2-PBM)

and PBM 454 (which we named NV3-PBM). Affinity was 10 times higher than that of the starting sequence (NV1-PBM) for NV2-PBM ($K_d$ of 120 nM) and 20 times higher for NV3-PBM ($K_d$ of 60 nM). The kinetics of binding for NV1-PBM (original sequence) and NV3-PBM (sequence with the highest affinity) were compared in stopped-flow experiments. For NV3-PBM, we were able to obtain an accurate value for the association rate constant ($1.4x10^7$ $M^{-1}.s^{-1}$, a 1.6-fold increase with respect to NV1-PBM). We could obtain estimates only for the very slow dissociation process, with an approximate dissociation rate constant of 0.89 $s^{-1}$, more than one order of magnitude higher than the corresponding values for the other peptides tested, such as the original PBM, PTEN-PBM (9.7 $s^{-1}$) and NV1-PBM (16.6 $s^{-1}$). The residence time of NV3-PBM on the MAST2-PDZ domain was 1.1 seconds, a value 10 times greater than that for the initial NV1-PBM sequence.

***Affinity profiles of the three NV sequences***

We addressed the issue of PDZ-NV-PBM specificities by performing automated holdup assays (20). We used this high-throughput chromatographic approach to quantify PDZ-PBM interaction affinities at equilibrium in solution for a collection of 222 human PDZ domains, corresponding to 83% of the original PDZome (266 PDZ domains) overexpressed in a soluble form. The holdup screens probing the interaction of the PDZome with NV1-, NV2- and NV3-PBM, were performed in triplicate. In Fig. 4, the PDZ binding intensities (BI) of NV-PBMs are ranked in descending order from left to right. Using a stringent BI threshold of 0.2 to retain only high-confidence binding pairs, the holdup assay identified 5, 8 and 15 hits for NV1-PBM, NV2-PBM and NV3-PBM, respectively. The PDZ domains recognized by NV1-PBM also bound to NV2-PBM. The NV2-PBM binders were also included in the set of proteins recognized by NV3-PBM. The number of binders detected increased with affinity for MAST2-PDZ, but the slope of BI decay in the binding profiles indicated that recognition specificity was roughly maintained from NV1-PBM to NV3-PBM. Furthermore, this affinity-based ranking demonstrated that all three NV-PBMs targeted MAST2-PDZ preferentially among the 222 PDZ domains tested.

***Comparison of the biological activities of NV constructs in NS cells***

Mini-G sequences encoding NV2-PBM or NV3-PBM were constructed as described (Fig. 5A). They were delivered to NS cells by lentivirus vectors. The viability of the three lentivirus vectors encoding NV1, NV2 and NV3 was demonstrated by quantifying NV transcripts in the transduced NS cells (Fig. 5B, left panel). Each viral vector produced similar amounts of the corresponding NV1, NV2 and NV3 polypeptides, as shown by WB (Fig. 5B, right panel). We then compared the effects on neurite outgrowth of NV1, NV2 and NV3 in NS cells, 72 h after transduction (Fig. 5C and Fig. S2 for NeuronJ drawings). Peptide rankings for the stimulation of neurite outgrowth (NV3>NV2>NV1) were identical to those obtained *in vitro* for affinity for MAST2-PDZ.

We then analyzed whether the greater capacity of NV3 and NV2 to stimulate neurite outgrowth was associated with a greater complexity of neurite arborization. We performed Sholl analysis (22) to determine how many times the neurites of a given cell crossed concentric circles of increasing radius centred on the cell soma. The results of the analysis are expressed as the mean number of neurites crossing each circle of increasing radius from 0 to 250 µm for NS cells transduced with each type of construct and for non-transduced cells (Fig. 5D). The expression of the various NVs was associated with a significant increase in neurite arborization complexity relative to that for non-transduced cells, even though the increase between arborization triggered by NV1 and NV2 stays modest. As already shown above for the neurite outgrowth phenotype, NV3 yielded the best increase in arborization.

***Practical impact on drug design*** The NVs were expressed in neurons *via* lentiviral vector transduction. However, this type of vectorization is not optimal for human therapeutic applications, thereby alternative way to deliver NV need to be considered. Peptide delivery is a possible option, only if two criteria are respected: a) the active sequence is coupled with a cell-penetrating molecule, CPM, to facilitate passage across the outer membrane of the neurons and b) the entire polypeptide size remains small to facilitate its production.

We reduced the size of the most active peptide NV3, by restricting the peptide to its cytoplasmic domain (NV3-Cyto). A new lentiviral vector, NV3-Cyto, was designed, to determine whether the removal of the part of the sequence responsible for endomembrane anchorage (the SP, two amino acids of the EC and the TM domain) could be tolerated (Fig. 6A). We assessed lentivector viability for NV3 and NV3-Cyto by performing RT-PCR on NS cells after transduction (Fig. 6B). NS cells transduced with NV3-Cyto displayed neurite outgrowth, but less than that observed with the parental peptide NV3 (Fig.6C). Unlike cells transduced with the parental peptide, the cells transduced with NV3-Cyto were unable to achieve higher levels of branching (data not shown). The properties of NV3-Cyto-transduced cells were similar to those of cells transduced with the initial construct, NV1 (as shown in Fig. 6C for neurite outgrowth and Fig. 6D for branching). Thus, NV polypeptides encoding the PBM sequence having a high affinity for MAST2-PDZ can still trigger neurite elongation, even if membrane anchorage is lost.

To directly deliver NV3-Cyto into neurons as a peptide, we coupled the NV3-Cyto construct and its control, NV3-CytoΔ, to a CPM, as displayed in Fig. 7A. We used the variable part (VHH) of a single-chain llama antibody as the CPM, because this molecule has been shown to cross the blood-brain barrier and the plasma membrane of brain cells (23,24). Constructs encoding CPM-NV3-Cyto and CPM-NV3-CytoΔ, as a control (CPM-Neurovita and CPM-NeurovitaΔ, respectively), were genetically engineered (Fig. 7A), expressed in bacterial periplasm and the resulting proteins were purified. We have previously shown that when CPM-Neurovita was added to a mixed culture of humans neurons, astrocytes and microglia CPM-Neurovita targets neurons preferentially (25). Here, we analyzed whether CPM-Neurovita could be detected in NS by WB or flow cytometry after CPM-Neurovita was added to the culture medium (Fig S3). Six hours after the addition of CPM-Neurovita to the culture medium, CPM-Neurovita could be detected by WB in the cell lysates at the expected molecular weight of 22.7 kDa (Fig. S3A). Thirty minutes after the addition of CPM-Neurovita to the culture medium, CPM-Neurovita entry was detected by flow cytometry when the cells had been previously permeabilized (Fig. S3B, left panel) whereas no staining was observed on non-permeabilized cells (Fig. S3B, right panel). This indicates that CPM-Neurovita associates with some cellular area made accessible to the antibody by the permeabilization treatment such as the cytoplasm or the submembrane area.

When added to the culture medium of NS cells, CPM-Neurovita (2.35 pg/cell) triggered stronger neurite outgrowth than the one observed for CPM-NeurovitaΔ-treated cells or non-treated cells (Fig. 7B). Time-lapse recordings over a period of 12 h (starting 18h to after treatment up to 30h post treatment) with Incucyte Technology were used to compare the speed of neurite growth. The number of neurites per neuron (Fig. 7C) and the speed of growth (Fig. 7D) were significantly greater in NS cells treated with CPM-Neurovita than in cells treated with CPM-NeurovitaΔ.

Thus, NV efficacy is qualitatively maintained when the NV sequence is delivered as a cell-penetrating interfering peptide.

**Discussion**

Protein-protein interaction domains including PDZ domains governing signaling pathways critical for cell homeostasis are emerging as promising targets for therapeutic applications (26-30). These signaling pathways can be manipulated with short interfering peptides, which disrupt these interactions. Viruses are obligate intracellular parasites, and their multiplication is dependent on cellular resources. The mimicry of PBM by viral proteins is a simple strategy by which several viruses take control of the cellular machinery. In particular, this mimicry enables some viruses to modify the commitment of infected cells to death or survival (16,31,32). Identification of the viral sequences involved and elucidation of their mechanisms of action could potentially facilitate the design of efficient interfering peptides. We have identified a viral protein, the RABV G-protein, that promotes neurite outgrowth by disrupting interactions between the PDZ of the MAST2 kinase and its endogenous ligands, such as PTEN, via its C-terminal PBM. In this study, we investigated whether we can leverage the robust strategy

evolved by a virus for ensuring its own propagation in the brain, to develop a short interfering peptide that promotes neurite outgrowth by specifically targeting MAST2-PDZ.

We hypothesized that NV peptides derived from the RABV G-protein and competing with the endogenous ligand for binding to the MAST2-PDZ domain would promote neurite outgrowth following their delivery into cells. We first showed that short peptides encoding the Cyto-domain of the G-protein reproduce the properties of RABV. However, the presence of certain parts of the viral RABV G-protein involved in association with endomembranes, such as the SP and TM domain, were necessary to insure their correct cellular targeting. The resulting interfering peptide, NV1, encodes a PBM bound to MAST2-PDZ with an affinity in the micromolar range similarly to PTEN, which is one of the endogenous ligands of MAST2-PDZ. We suggested that increasing the affinity of the interfering peptide for MAST2-PDZ would increase the peptide potency to stimulate neurite outgrowth. We used structural, kinetic and thermodynamic data for a large number of PDZ/peptide complexes to design peptides with a higher affinity for MAST2-PDZ, with the viral and one endogenous partners of MAST2 (*i.e.* RABV G-protein and PTEN) as the starting material. One of the original features of our approach relates to the specificity of MAST2-PDZ recognition. In addition to increasing the affinity of NV peptides for MAST2-PDZ, we also wished to maintain this specificity for MAST2-PDZ to prevent undesirable additional interactions with other endogenous proteins. PDZ binding selectivity seems to have been achieved throughout evolution (33,34). Extensive scans of random peptides against a large collection of PBM domains led to the definition of discrete sets of PDZ classes, conserved from worms to humans, encompassing the last seven amino-acid residues of potential PBM candidates (35). Most attempts to improve the strength of a given PDZ-PBM interaction have focused on modifications to the pre-existing stretch of seven amino-acid residues at the C-terminus of the PBM, position by position. Such efforts have generally resulted in a loss of the specificity of this interaction pair with respect to competing PDZ or PBM molecules (16,36-38). Indeed, we previously showed that one mutation at position -3 in the PBM sequence of the RABV G-protein is sufficient to extend cellular protein recognition patterns and to switch cell fate from survival to death (16). We therefore decided to keep the COOH terminus QTRL> intact in the new NVs.

Some PDZ domains make use of amino-acid sequences beyond the canonical PDZ domain fold, which are referred to as extended PDZ domains. Similarly, some PDZ ligands require extension sequences beyond the C-terminal PBM, including some more than 10 residues from the last C-terminal residue, for complex formation with the PDZ domain of the partner protein (38). We have shown that both RABV G-protein and PTEN make use of a PBM extension up to position -12 for binding to MAST2-PDZ (18,19). The unusually large interaction interface between MAST2-PDZ and G-protein or the PTEN C-terminus involves not only the four-amino acid canonical PBM, but also a two-amino acid N-terminal anchor (SW and PF for G-protein and PTEN, respectively). This N-terminal anchor increases MAST2 – PDZ binding affinity and probably plays a crucial role in narrowing the specificity of interaction between MAST2 and its partners (18). This finding is reminiscent of observations from other studies indicating that PTEN also uses an N-terminal extension to bind the third PDZ domain of PAR-3, improving the specificity of PTEN for its target and its subcellular distribution at the junctional membrane of polarized cells (39). We suggested that in this case, the N-terminal anchor might be involved in PBM-PDZ specificity and might increase the affinity of the PBM for MAST2-PDZ. We therefore did not modify this part of the molecule either.

By conserving the two viral anchoring sites, $_{NH2}$SW- and –QTRL$_{COOH}$, from virulent RABV strains, which promote neuron survival, we were able to conserve the specificity of NV peptides for MAST2-PDZ, as illustrated by high-throughput PDZome screening.

We increased the affinity of NV peptides for MAST2-PDZ mostly by decreasing the entropic cost of binding by modulating the flexibility of the central linker connecting the two binding sites of NV peptides, thereby greatly increasing the residence time of NV on MAST2-PDZ.

After two rounds of optimization, we obtained peptides with an affinity 20 times higher ($K_D$=60 nM) than that of the initial viral or endogenous peptides (1 300 nM). Such an affinity, in the nanomolar range, is particularly high for a PDZ/ligand system, especially for molecules targeting a single PDZ domain. For example, interfering peptides targeting the Disheveld PDZ and functioning as an inhibitor of the Wnt/beta-catenin signaling pathway or targeting the PDZ1 of PSD95 and functioning as an inhibitor of nitric oxide (NO) synthesis, have $K_d$ values in the micromolar range (40-42). A few examples of nanomolar affinity (3-16 nM) have been reported for multivalent inhibitors targeting multi-PDZ containing proteins, such as those targeting proteins of the MAGUK family (43).

The selected peptides, NV 1, 2 and 3, are capable of inducing the neurite outgrowth of NS cells with an efficiency related to their affinity for MAST2-PDZ. These data strongly support our hypothesis that NVs activity can be increased by enhancing the strength of interaction with the cellular partner.

Given their capacity to promote neuron survival, NVs could have therapeutic applications for diseases of the nervous system in which neuron survival is compromised. The different ways to deliver NVs will be determined by the nature of the disease. For chronic diseases, it may be advantageous to deliver NVs in gene form, via a viral vector, such as a lentivirus or an adeno-associated virus (AAV), which can transduce neurons. The delivery of a peptide, rather than a gene, may be more appropriate when a fast mode of action is required for example in the case of an acute nerve injury. We therefore tried to adapt NV sequences for peptide production, by reducing the peptide size, to facilitate production and delivery.

We showed that for the optimized peptide NV3 that the processing and translocation were dispensable. Thereby, we were able to halve the size of the peptides, while maintaining the activity of the original construct. However, the 20-fold improvement in affinity initially achieved was counterbalanced by imperfections of targeting. This design was feasible only for NV3, the peptide with the highest affinity for the target. Indeed, our first attempt to generate a similar construct from the NV1 peptide resulted in a total loss of neurite outgrowth stimulation (data not shown). We subsequently demonstrated the feasibility of replacing the viral vector delivery system by fusing a shortened NV3 peptide to a CPM.

In this study, resulting from a combination of biophysical and cellular approaches, we showed for the first time that a virus-derived peptide could be optimized to trigger neurite outgrowth, in several types of neurons. This work opens up a number of very promising perspectives for the use of NV as a potential drug candidate in neurodegenerative diseases.

## Experimental procedures

### *Cell lines, plasmids encoding RABV G-protein sequences, lentivectors and CPM-Neurovita*

Neuroscreen cells (NS), a subclone of rat pheochromacytoma 12, PC12, neuronal cells, were obtained from Cellomics (USA) and cultured according to the supplier's instructions. NS cells were grown in non-differentiating (NDF) medium (Roswell Park Memorial Institute 1640, RPMI 1640 medium, Thermo Fisher Scientific France #11875093; 5% foetal bovine serum, FBS; 10% horse serum; 1% 200 mM glutamine, Thermo Fisher Scientific France #25030149 and 1% 100 x Penicillin Streptomycin, Pen-Strep, Thermo Fisher Scientific France #15140148). The differentiating (DF) medium had the same composition with the addition of 200 ng/ml of nerve growth factor (NGF; SIGMA USA #N2513). A clone of the human SH-SY5Y neuroblastoma cell line, which was originally used to decipher the role of the kinome, including the role of MAST2, in neurite outgrowth, was obtained from Dr S.H. Loh and was grown as previously described (12). The NDF for these cells consisted of Dulbecco's Modified Eagle Medium 12, DMEMF12 (Thermo Fisher Scientific France # 31330038) supplemented with 10% FBS plus 1% 100 x Pen-Strep and 1% 200 mM glutamine. The DF medium for these cells was Neurobasal medium (Thermo Fisher Scientific France #21103049) supplemented with B27 medium (Thermo Fisher Scientific France #A3582801), 1% 100 x Pen-Strep, and 1% 200 mM glutamine and 1 mM db-cAMP (Sigma-Aldrich USA #D06627).

Cortical neurons were prepared from E16 Swiss mice as described by S. Vitry *et al*. (44). Embryonic mouse brains were dissected in Hank's Balanced Salt Solution, HBSS (Life Technologies #14175) supplemented with 10 mM Hepes, 4-(2-hydroxyethyl)-1-piperazineethanesulfonic acid, (Life Technologies #15630), 0.05% glucose (Sigma #G8769) and 50 µg/ml gentamicin (Life Technologies #15750). Meninge-free brain cortices were collected in HBSS supplemented with 400 U/ml DNAse (Roche #04536282001) and incubated with the Liberase HD enzymatic cocktail (Sigma #5401054001). The digested tissues were triturated mechanically and the enzymatic reaction was stopped by adding FBS. The suspension was washed in HBSS and centrifuged for 5 min at 200 x *g*, and the resulting cell pellet was suspended in Neurobasal medium (Life Technologies #21103) supplemented with 25 nM 2-mercaptoethanol (Sigma #M7522), 50 µg/ml gentamicin, 5 mM Hepes, 2 mM Glutamax (Life Technologies #35050), N2 (Life Technologies #17502) and B27 (Life Technologies #17504). Viable cells were used to seed the wells at a density of $10^4$ to 3 x $10^4$ cells per $cm^2$ on plates coated with poly-D-lysine (Sigma #P6407) and laminin (Sigma #L2020). The cells were allowed to sediment, and to adhere for 20 min at room temperature. They were then transferred to an incubator containing 9% $CO_2$ in air maintained at 37°C, for 40 min, before the addition of 10 µg/ml fluodeoxyuridine (Sigma #F0503) and 25 µg/ml uridine (Sigma #U3003).

The iPSc clones (clone 2.1, (45) and clone 3.1, unpublished) were stimulated to differentiate into motor neurons as described by Maury *et al*. (46).

The G-[SP-(2aa)-TM-Cyto] plasmid, which encompasses all the protein domains of the full-length RABV G-protein (RABVvir strain) 2 (signal peptide SP, transmembrane TM, cytoplasmic domain Cyto and the two amino acids (2aa) flanking the TM), was described in patent application WO2010/116258 (47). The nucleotide sequences of NV1, NV1Δ, NV2 and NV3 were obtained by PCR and inserted into the pLenti6.3/V5-TOPO® (Blasticidin) or pLenti7.3/V5-TOPO® (e-GFP) vector with the TA cloning kit (Invitrogen France # K5315-20). Lentiviruses were produced in 293T cells by standard procedures, as described by Zufferey R. *et al.* (48). The number of HIV particles was determined with the HIV p24 ELISA kit (Perkin Elmer USA # NEK 050B). The infectivity of recombinant lentivectors was systematically monitored by RT-qPCR and/or flow cytometry. The GenBank accession numbers of the lentivectors are: Lenti-NV1 (KJ742386), Lenti-NV1Δ (KJ742387), Lenti-NV2 (MH197113) and Lenti-NV3 (MH197112). The CPM-Neurovita) and its PBM-deleted counterpart (CPM-NeurovitaΔ) were described in European patent application EP14306388(49).

CPM-Neurovita is a 209aa long (MW =22.7kDa) chimeric molecule consisting of i) Neurovita and ii) a CPM formed by a Neuro-Tag domain (a RABV-derived peptide from the RABVvirG-Protein ectodomain that recognizes the AChR Alpha 7 subunit), and by the variable part (VHH) of a llama single-chain antibody capable of crossing biological membranes and the blood brain barrier (23), and iii) a StrepTag sequence to label the molecule. CPM-NeurovitaΔ is the disabled form of the molecule with a deletion of the last 4 aa of the PBM. The GenBank accession numbers are KJ784393 (CPM-Neurovita) and KJ784394 (CPM-NeurovitaΔ). The genes were synthesized chemically (MWG Operon, Germany) and inserted into the pASK-IBA2 plasmid (IBA, BioTAGnology, Germany) under the control of the tetracycline promoter. The ompA signal sequence added by this plasmid directs the expressed protein into the periplasmic space of the bacteria and is cleaved during translocation. The recombinant plasmids were used to transform XL1-blue *E. coli* bacteria (Stratagene, USA). Recombinant bacteria were identified by PCR and glycerol stocks were generated. CPM-Neurovita peptides were expressed and purified from the bacterial periplasm as described by Lafaye *et al*. (50). The periplasmic extract was further purified by immunoaffinity chromatography with a mouse high-affinity anti-StrepTag IgG1 mAb, C23.21 (kindly provided by Pierre Lafaye). The molecules were stored in 0.25 x PBS at -80°C. CPM expression was monitored by western blotting with the C23.21 mAb, with quantification by Odyssey Li-Cor infrared chemo luminescence (Li-Cor, USA) with a standardized VHH-StrepTag preparation.

***Neurite outgrowth***

SH-SY5Y and NS cells: Neurite outgrowth assays on SH-SY5Y and NS were performed as described in detail by Loh S.H. *et al.* (12) and Prehaud C. *et al*. (16). Briefly, SH-SY5Y or NS cells were used to seed 24-well plates (CellBind plastic ware, Corning USA # 83-3337) containing non-differentiating medium, at a density of 40 000 cells per well. They were cultured overnight at 37°C. The medium was then replaced with DF medium and the cells were incubated for a further 6 h. They were then infected with 30 ng p24 lentiviral vector or treated with 2.35 pg/cell CPM-Neurovita or CPM-NeurovitaΔ in DF medium for 1 h. The cells were washed once with DF medium, and incubated in DF medium for 24 h at 37°C. Thirty hours (SH-SY5Y) or 72 h (NS) post transduction, the cells were fixed by incubation with 3% paraformaldehyde (PFA) in phosphate-buffered saline (PBS, Thermo Fisher Scientific France # 14040141) for 20 min at room temperature and treated for 5 min with 0.1% Triton-X-100 and 50% normal goat serum (NGS) in PBS. Neuron-specific anti-βIII-tubulin antibody (Promega France # G7121) and Hoechst 33342 (Thermo Fisher Scientific France #62249) were used to stain the neurite processes and the nuclei, respectively. Alternatively, the cells were also stained with crystal violet, which preserves the neurite processes. SH-SY5Y human neuroblastoma cells (30 fields, mean of 300 cells per field) and NS cells (36 fields, mean of 324 cells per field) were imaged with a Leica DM 5000B UV microscope equipped with a DC 300FX camera (x40 or x20 objective). The images were analyzed using ImageJ 1.38X Software (Wayne Rasband, NIH, USA, http://rsb.info.nih.gov/ij/) and its plug-in NeuronJ (51) (http://www.imagescience.org/meijering/software/neuronj/). The effects of bias were minimized by performing the experiment blind, with relabeling of the samples.

Motor neurons. Motor neurons were plated at a density of 10 000 cells per well (48-well plates). Gene transfer was performed with lentiviral vectors (six ng p24 per well) after the next day.

Transduction was obtained in 80-90% of cells. Non-treated conditions was used as a quality control of the culture. Cells were fixed three days later (4% PFA in PBS for 20 min at room temperature). The cells were washed in PBS and incubated for 1 h at room temperature in PBS containing 2% NGS, 1% bovine serum albumin (BSA, SIGMA USA # A2153) and 0.1% Triton X-100 (SIGMA USA # X100). Cells were then incubated overnight at 4°C with anti-βIII-tubulin antibody (TUBB3, Biolegend France # 801201), washed three times in PBS and incubated for 1 h at room temperature with Alexa Fluor 555-conjugated anti-mouse IgG2a antibody (Thermo Fisher Scientific # A-21137). Nuclei were stained with 1 mg/ml Hoechst H33342 (Thermo Fisher Scientific France #62249). Motor neurons (500 cells) were analyzed with the Cell Insight platform (Cellomics, Thermo Fisher Scientific France), using the Neuronal Profiling Bio-application suite. Neurite outgrowth phenotype was determined in triplicate experiments.

Mouse cortical neurons. Mouse cortical neurons (3DIV) were plated on 96-well dark-sided cell-binding plates (Corning USA #3340). They were infected with 10 ng p24/well of lentiviral vector 2 h after seeding. The medium was changed 12 h after infection. Three days post infection, the medium was carefully removed and the neurons were fixed by incubation with 4% PFA for 20 min at room temperature. Plates were washed three times with PBS and the cells were permeated by incubation with 0.3 % Triton X-100 (SIGMA USA # X100) for 10 min at room temperature. Analysis of neuronal βIII tubulin immunofluorescence and Hoechst staining were performed as described above for SH-SY5Y/NS cells. Primary cortical neurons (10 fields, mean of 650 cells per field) were analysed with the Cell Insight platform (Cellomics, Thermo Fisher Scientific France), using the Neuronal Profiling Bio-application suite. Neurite outgrowth phenotype was determined in triplicate experiments.

***Time-lapse experiments in NS cells***

We determined the neurite-bearing cell phenotype and assessed the speed of neurite outgrowth by using NS cells in NDF to seed collagen-coated 24-well plates (CellBind plastic ware, Corning USA # 83-3337) at a density of 40 000 cells per well. The cells were cultured overnight at 37°C. The NDF medium was replaced by DF medium containing only 10 ng/ml of NGF and 7% FBS (52), 24 h after seeding, and the cells were incubated for a further 3 h. They were then treated with 700 ng/well CPM-Neurovita or CPM-NeurovitaΔ in

DF medium. Cells were incubated in DF medium for 48 h at 37°C, under an atmosphere containing 5% $CO_2$ in an IncuCyte Live-Cell analysis system. Images were recorded every hour over a two-day period. For live-cell imaging on IncuCyte, NS cells (nine fields mean of 43 cells per field) were recorded on bright-field images and analyzed with Fiji/ImageJ (https://fiji.sc/) and the NeuronJ plug-in. The percentage of neurite-bearing cells (53) and the speed of neurite outgrowth and elongation were monitored over 12 h, from 18 to 30 h after treatment.

***Arborization analysis***

Sholl analysis (22,54) was used to assess dendritic arborization. This analysis was performed as described by Sahay A. *et al*. (22) and Lioy DT. *et al*. (55). Measurements were obtained from 8-bit converted images with the Sholl analysis plugin of Neuron J. (http://www-biology.ucsd.edu/labs/ghosh/software/). Branching complexity was quantified by counting the intersection of neurites with each of 10 concentric circles of increasing radius drawn around the cell body. We picked 30 neurons at random from each group for analysis. Experiments were performed at least three times. Bias was minimized by performing the experiments blind after sample relabeling.

***Reverse transcription and quantitative polymerase chain reaction***

The procedures used for reverse transcription and quantitative polymerase chain reaction (RT-qPCR) have been described elsewhere (56). Basically, cDNA was synthesized from 1 µg total RNA with the SuperScript II reverse transcriptase (Thermo Fisher Scientific France #18064014). Quantitative real-time RT-PCR (RT-qPCR) was performed in triplicate with an ABI Prism 7500 fast sequence detector system with GoTaq PCR master mix (Promega France #M7133). After normalization against 18S rRNA, the relative abundance of mRNA was obtained by calculating the difference in threshold cycles between the test and control samples (mock value set at 1), as according to the $\Delta\Delta C_T$ method. The primers used were

Lenti-1 (AGACGCCATCCACGCTGTTTTGACCTCCATAG),

Lenti-2 (CCAAAACACAATGGAAAAACCAGAAGGGGTAC),

Lenti-3 (GTGTTGCGTAGGTTCTGATCGATTGACTCTTC),

18S (F: CTT AGA GGG ACA AGT GGC G; R: ACG CTG AGC CAG TCA GTG TA)

MAST2: Quantitect primers (Qiagen, Germany) QT00042574.

***Western blotting (WB)***

Proteins were suspended in Radio Immunoprecipitation Assay, RIPA, buffer (Sigma USA #R0278) supplemented with Complete ULTRA EDTA (Roche USA #05892970001), PhosSTOP (Roche USA #04906845001) and nuclease (Thermo Fisher Scientific France #88701). Protein extracts were diluted in NuPAGE LDS buffer (Thermo Fisher Scientific France #NP0007) containing NuPAGE reducing agent (Thermo Fisher Scientific France #NP0004). Protein samples (15 µg/µl) were then loaded onto NuPAGE Novex 12% Bis-Tris gels (Thermo Fisher Scientific France #NP0341) and subjected to electrophoresis in MOPS SDS running buffer (Thermo Fisher Scientific France #NP0001). The protein bands were blotted onto PVDF Immobilon-FL membranes (Millipore France #IPFL00010). Membranes were blocked with 5% BSA in PBS-T buffer (PBS with 0.1% Tween 20) and incubated overnight at 4°C with the primary antibody in blocking buffer containing 0.1% Tween 20 (SIGMA USA #P1379). The membrane was washed with 0.1% Tween 20 in PBS and the antigen/antibody complex was detected with a horseradish peroxidase (HRP)-conjugated secondary antibody. Membranes were washed with PBST and visualized with the ECL western blot kit (Thermo Fisher Scientific France #35055) on a G-Box (SYNGENE USA). The primary antibodies were the anti-βIII-tubulin (Promega France # G7121) and an anti-RABV G-cyto domain (produced in-house, NIV biological

collection) antibody. The secondary antibody was an HRP-conjugated anti-mouse IgG antibody (GE Healthcare U.K. #NA9310).

***MAST2 immunofluorescence in NS or SH-SY5Y cells***

Neuronal cells were seeded on Poly-L-lysine-Collagen coated glass slide (3e+04 cells per slide) in a 24-wells cell culture plate. Twenty-four hours later, cells were rinsed with PBS buffer (3 times) and fixed with 100% methanol at -20°C for 20 min. Then cells were washed three times with PBS, blocked with 5% goat serum in PBS for an hour at room temperature, rinsed three times with PBS and incubated overnight at 4°C with the anti-MAST2 antibody (1/500, Thermo Fisher Scientific France #PA5-75974) diluted in 5% goat serum in PBS. The day after, the glass slides were washed three times with PBS, incubated with the secondary antibody conjugated with AF555 (1/500, Thermo Fisher Scientific France #A27039) and Hoescht 33342 (Thermo Fisher Scientific France #H3570) for one hour at room temperature. Then the slides were washed three times with PBS and mounted with prolong gold (Thermo Fisher Scientific France #P36982). Cells were imaged with a Zeiss LSM70 confocal UV microscope.

***Penetration of CPM-Neurovita in NS***

The flow cytometry procedures, have been described in Prehaud *et al*. (47,57). Briefly, NGF-treated (6 hours) NS cells which had been seeded on 6 well plates (0.5.e+06 cells per well) were treated with 20 ng of CPM-Neurovita or mock-treated with PBS buffer for 30 min at 4°C. Then, cells were washed 3 times with PBS buffer before to be permeabilized to detect both the molecules bound to the membrane and the molecules in the cytoplasm. The CPM-Neurovita molecules were detected with an anti-strep Tag mAb C23.2 (IP collection, Dr Pierre Lafaye) plus a Cy5 conjugated anti-mouse antibody (Jackson laboratory, USA).

For WB analyses, 1e+06 NS cells cultivated in NDF medium were processed as above after being treated with 9 µg of CPM-Neurovita or mock-treated with PBS buffer for 6 hours at 37°C. Then cells were washed 3 times with PBS buffer, lysed with RIPA buffer and processed for WB using the anti-strep tag antibody C23.2.

**MAST2-silencing**

SH-SY5Y were silenced for the expression of *MAST2* by using specific lentiviral shRNA MAST2 (TRCN0000001733, TRCN0000001735 and TRCN0000001736) and pL.KO1shRNA (RHS4080) as control. The lentiviral shRNA were found among the collection of the Open Biosystems Expression Arrest™ TRC library (Broad Institute MIT and Harvard, USA, sold by Thermofisher). Lentiviral shRNA viral stocks were produced as previously described. Briefly, SH-SY5Y (74 x $10^6$ cells in 12ml of medium) were infected with 900ng of p24 equivalent of each lentiviral shRNA vector stock for two days. Then an aliquot of the cells was taken, total RNA was extracted and gene expression was monitored by Q-RTPCR. Neurite outgrowth was assayed in cultures exhibiting a knockdown of expression of >80%. Silencing experiment was conducted on triplicate individual samples.

**Statistical analysis**

ANOVA with Bonferroni's multiple comparison post hoc-test and student's T test were conducted with Graph Pad Prism version 7 or 8 software.

***Sample preparation for biophysical methods***

MAST2–PDZ was expressed and purified as previously described (58). PBM peptides were synthesized on solid-phase supports, with the Fmoc (9-fluorenyl methoxycarbonyl) strategy (ProteoGenix; see Fig. 3B for sequences). All biophysics experiments were performed in 50 mM Tris/HCl, 150 mM NaCl at pH 7.5.

***Isothermal titration microcalorimetry***

ITC measurements were performed as previously described (16) with VP-ITC and ITC200 calorimeters (Malvern). MAST2-PDZ (10 to 30 µM) was titrated at 298 K by 20 to 45 consecutive injections of 2 to 7 µl aliquots of the peptides (110 to 280 µM). Raw data were normalized and corrected for the heats of dilution of the peptides. Equilibrium dissociation constants were determined by fitting nonlinear curves to the corrected based on a model with one set of sites, with Origin7.0 software (OriginLab).

***Stopped-flow experiments***

The kinetics of association between MAST2–PDZ and the NV3 peptide were studied at 20°C with SFM300 stopped-flow equipment with fluorescence detection (BioLogic). Typically, 150 µl of MAST2–PDZ solution was rapidly mixed with an equal volume of peptide solution. For each peptide, three concentrations (2.5, 5 and 10 µM) were tested at a constant MAST2–PDZ–peptide ratio of 1:10 to respect pseudo-first-order conditions. The maximal concentration of MAST2–PDZ was 1 µM. A mixing time of 15 ms was used (total flow rate of 20 $ml \cdot s^{-1}$), resulting in a dead time of 2.5 ms. Data points recorded between 0 and 3 ms were excluded from the fitting process. The flow cell was illuminated with a monochromatic UV light at 295 nm (bandwidth 8 nm) and emitted fluorescence was collected perpendicularly to the incident beam through a 325 nm high-pass filter. Kinetic data were acquired and analyzed as previously described (18). We stored and processed 10-12 averaged traces independently. Averaged kinetic traces from stopped-flow experiments were fitted independently with the following mono-exponential equation: $F(t)=A \cdot e^{-kobs \cdot t}$ + offset. For each peptide concentration, the mean values of amplitude, the observed rate constant and the corresponding SDs were calculated from the fitted values deduced from each series of averaged kinetic data. Intrinsic association and dissociation rate constants, *k*on and *k*off, were determined from the linear regression of the variation of *k*obs as a function of peptide concentration.

***Hold-up***

As described by Vincentelli R. *et al*. (20), 222 PDZ domains clones from a complete collection of 266 PDZome clones were successfully expressed. The automated holdup assay protocol was performed on a Tecan freedom Evo200 machine with 384-well plates. A 41 µM stock solution of biotinylated Neurovita peptide fixed on streptavidin beads was incubated with a 4 µM His-MBP-PDZ domain solution. After incubation, the liquid phase of the plates was collected and filtered and the concentration of unbound PDZ domains in the filtered flow-throughs was measured by microfluidic capillary gel electrophoresis with a LabChip GX II machine (Caliper, PerkinElmer). Binding intensities (BIs) were calculated as described in the supplementary data of the paper by Vincentelli R. *et al*. (20).

**Acknowledgments**

This work was supported by the following grants: **ANR (Agence Nationale de la Recherche),** BSV8-0008-01 *MAST-2-PTEN*. **AFM (Association Française contre les Myopathies)** *Characterization of pathological defects in motor neurons derived from patients Amyotrophic Lateral Sclerosis (ALS).* ***Grand Prix de l'Académie des Sciences/Fondation Générale de Santé,*** and Incentive grant from **Institut Carnot-Pasteur Maladies Infectieuses** *Unraveling the neuroprotective functions and optimization of new neuroprotective compound*. The research leading to the results on IPSC has received funding from the programs **Investissements d'Avenir ANR-10-IAIHU-06** and **ANR-11-INBS-0011-NeurATRIS**: Translational Research Infrastructure for Biotherapies in Neurosciences. ET and FD are recipients of PhD fellowships from the Ministère de l'Enseignement Supérieur et de la Recherche. C L-O was supported by a PhD fellowship from Revive (ANR-10-LABX-73).
We thank Sylviane Hoos (Biophysics Core, Institut Pasteur) for ITC expertise and the team of the Technology Core of the Center for Translational Science (CRT), Institut Pasteur, for their help our with the Incucyte Technology.

**Conflict of interest statement**:

KZ, LM, PC, TE, VS and WN are co-inventors of the two following patents:

Prehaud C, Lafon M, Wolff N, Khan Z, Terrien E and Vitry S are co-inventors of Institut Pasteur patent "High MAST2-affinity polypeptides and uses thereof". PCT/EP2012/072073, WO2013068430, European patent 11 306 454.7.

Prehaud C and Lafon M are co-inventors of Institut Pasteur Patent "Nanobodies suitable for neuron regeneration therapy". PCT/EP2015/070669. EP14306388.1.

### *References*


1. Datta, S. R., Brunet, A., and Greenberg, M. E. (1999) Cellular survival: a play in three Akts. *Genes Dev* **13**, 2905-2927
2. Brunet, A., Bonni, A., Zigmond, M. J., Lin, M. Z., Juo, P., Hu, L. S., Anderson, M. J., Arden, K. C., Blenis, J., and Greenberg, M. E. (1999) Akt promotes cell survival by phosphorylating and inhibiting a Forkhead transcription factor. *Cell* **96**, 857-868
3. Knafo, S., and Esteban, J. A. (2017) PTEN: Local and Global Modulation of Neuronal Function in Health and Disease. *Trends Neurosci* **40**, 83-91
4. Zhang, Y., Granholm, A. C., Huh, K., Shan, L., Diaz-Ruiz, O., Malik, N., Olson, L., Hoffer, B. J., Lupica, C. R., Hoffman, A. F., and Backman, C. M. (2012) PTEN deletion enhances survival, neurite outgrowth and function of dopamine neuron grafts to MitoPark mice. *Brain* **135**, 2736-2749
5. Gregorian, C., Nakashima, J., Le Belle, J., Ohab, J., Kim, R., Liu, A., Smith, K. B., Groszer, M., Garcia, A. D., Sofroniew, M. V., Carmichael, S. T., Kornblum, H. I., Liu, X., and Wu, H. (2009) Pten deletion in adult neural stem/progenitor cells enhances constitutive neurogenesis. *J Neurosci* **29**, 1874-1886
6. Wyatt, L. A., Filbin, M. T., and Keirstead, H. S. (2014) PTEN inhibition enhances neurite outgrowth in human embryonic stem cell-derived neuronal progenitor cells. *J Comp Neurol* **522**, 2741-2755
7. Zhang, X. C., Piccini, A., Myers, M. P., Van Aelst, L., and Tonks, N. K. (2012) Functional analysis of the protein phosphatase activity of PTEN. *Biochem J* **444**, 457-464
8. Kwon, C. H., Luikart, B. W., Powell, C. M., Zhou, J., Matheny, S. A., Zhang, W., Li, Y., Baker, S. J., and Parada, L. F. (2006) Pten regulates neuronal arborization and social interaction in mice. *Neuron* **50**, 377-388
9. Markus, A., Zhong, J., and Snider, W. D. (2002) Raf and akt mediate distinct aspects of sensory axon growth. *Neuron* **35**, 65-76
10. Drinjakovic, J., Jung, H., Campbell, D. S., Strochlic, L., Dwivedy, A., and Holt, C. E. (2010) E3 ligase Nedd4 promotes axon branching by downregulating PTEN. *Neuron* **65**, 341-357
11. Chow, D. K., Groszer, M., Pribadi, M., Machniki, M., Carmichael, S. T., Liu, X., and Trachtenberg, J. T. (2009) Laminar and compartmental regulation of dendritic growth in mature cortex. *Nat Neurosci* **12**, 116-118
12. Loh, S. H., Francescut, L., Lingor, P., Bahr, M., and Nicotera, P. (2008) Identification of new kinase clusters required for neurite outgrowth and retraction by a loss-of-function RNA interference screen. *Cell Death Differ* **15**, 283-298
13. Valiente, M., Andres-Pons, A., Gomar, B., Torres, J., Gil, A., Tapparel, C., Antonarakis, S. E., and Pulido, R. (2005) Binding of PTEN to specific PDZ domains contributes to PTEN protein stability and phosphorylation by microtubule-associated serine/threonine kinases. *J Biol Chem* **280**, 28936-28943
14. Lachyankar, M. B., Sultana, N., Schonhoff, C. M., Mitra, P., Poluha, W., Lambert, S., Quesenberry, P. J., Litofsky, N. S., Recht, L. D., Nabi, R., Miller, S. J., Ohta, S., Neel, B. G., and Ross, A. H. (2000) A role for nuclear PTEN in neuronal differentiation. *J Neurosci* **20**, 1404-1413
15. Stambolic, V., Suzuki, A., de la Pompa, J. L., Brothers, G. M., Mirtsos, C., Sasaki, T., Ruland, J., Penninger, J. M., Siderovski, D. P., and Mak, T. W. (1998) Negative regulation of PKB/Akt-dependent cell survival by the tumor suppressor PTEN. *Cell* **95**, 29-39

16. Prehaud, C., Wolff, N., Terrien, E., Lafage, M., Megret, F., Babault, N., Cordier, F., Tan, G. S., Maitrepierre, E., Menager, P., Chopy, D., Hoos, S., England, P., Delepierre, M., Schnell, M. J., Buc, H., and Lafon, M. (2010) Attenuation of rabies virulence: takeover by the cytoplasmic domain of its envelope protein. *Sci Signal* **3**, ra5
17. Seo, W., Prehaud, C., Khan, Z., Sabeta, C., and Lafon, M. (2017) Investigation of rabies virus glycoprotein carboxyl terminus as an in vitro predictive tool of neurovirulence. A 3R approach. *Microbes Infect* **19**, 476-484
18. Delhommel, F., Chaffotte, A., Terrien, E., Raynal, B., Buc, H., Delepierre, M., Cordier, F., and Wolff, N. (2015) Deciphering the unconventional peptide binding to the PDZ domain of MAST2. *Biochem J* **469**, 159-168
19. Terrien, E., Chaffotte, A., Lafage, M., Khan, Z., Prehaud, C., Cordier, F., Simenel, C., Delepierre, M., Buc, H., Lafon, M., and Wolff, N. (2012) Interference with the PTEN-MAST2 interaction by a viral protein leads to cellular relocalization of PTEN. *Sci Signal* **5**, ra58
20. Vincentelli, R., Luck, K., Poirson, J., Polanowska, J., Abdat, J., Blemont, M., Turchetto, J., Iv, F., Ricquier, K., Straub, M. L., Forster, A., Cassonnet, P., Borg, J. P., Jacob, Y., Masson, M., Nomine, Y., Reboul, J., Wolff, N., Charbonnier, S., and Trave, G. (2015) Quantifying domain-ligand affinities and specificities by high-throughput holdup assay. *Nat Methods* **12**, 787-793
21. Terrien, E. (2012) Implication de la kinase MAST2 et de la phosphatase PTEN dans la survie neuronale induite par la glycoprotéine du virus de la rage. *PhD Thesis, Paris 6 University*
22. Sahay, A., Scobie, K. N., Hill, A. S., O'Carroll, C. M., Kheirbek, M. A., Burghardt, N. S., Fenton, A. A., Dranovsky, A., and Hen, R. (2011) Increasing adult hippocampal neurogenesis is sufficient to improve pattern separation. *Nature* **472**, 466-470
23. Li, T., Vandesquille, M., Bay, S., Dhenain, M., Delatour, B., and Lafaye, P. (2017) Selection of similar single domain antibodies from two immune VHH libraries obtained from two alpacas by using different selection methods. *Immunol Lett* **188**, 89-95
24. Li, T., Bourgeois, J. P., Celli, S., Glacial, F., Le Sourd, A. M., Mecheri, S., Weksler, B., Romero, I., Couraud, P. O., Rougeon, F., and Lafaye, P. (2012) Cell-penetrating anti-GFAP VHH and corresponding fluorescent fusion protein VHH-GFP spontaneously cross the blood-brain barrier and specifically recognize astrocytes: application to brain imaging. *FASEB J* **26**, 3969-3979
25. da Costa, A., Prehaud, C., Bakoa, F., Afonso, P., Ceccaldi, P. E., Lafaye, P., and Lafon, M. (2019) A Human Blood-Brain Interface Model to Study Barrier Crossings by Pathogens or Medicines and Their Interactions with the Brain. *J Vis Exp*
26. Fujii, N., Haresco, J. J., Novak, K. A., Stokoe, D., Kuntz, I. D., and Guy, R. K. (2003) A selective irreversible inhibitor targeting a PDZ protein interaction domain. *J Am Chem Soc* **125**, 12074-12075
27. Bach, A., Pedersen, S. W., Dorr, L. A., Vallon, G., Ripoche, I., Ducki, S., and Lian, L. Y. (2015) Biochemical investigations of the mechanism of action of small molecules ZL006 and IC87201 as potential inhibitors of the nNOS-PDZ/PSD-95-PDZ interactions. *Sci Rep* **5**, 12157
28. Khan, Z., and Lafon, M. (2014) PDZ domain-mediated protein interactions: therapeutic targets in neurological disorders. *Curr Med Chem* **21**, 2632-2641
29. Mo, S. F., Liao, G. Y., Yang, J., Wang, M. Y., Hu, Y., Lian, G. N., Kong, L. D., and Zhao, Y. (2016) Protection of neuronal cells from excitotoxicity by disrupting nNOS-PSD95 interaction with a small molecule SCR-4026. *Brain Res* **1648**, 250-256
30. Wu, Q. J., and Tymianski, M. (2018) Targeting NMDA receptors in stroke: new hope in neuroprotection. *Mol Brain* **11**, 15
31. Javier, R. T., and Rice, A. P. (2011) Emerging theme: cellular PDZ proteins as common targets of pathogenic viruses. *J Virol* **85**, 11544-11556
32. Lafon, M. (2011) Evasive strategies in rabies virus infection. *Adv Virus Res* **79**, 33-53

33. Stiffler, M. A., Chen, J. R., Grantcharova, V. P., Lei, Y., Fuchs, D., Allen, J. E., Zaslavskaia, L. A., and MacBeath, G. (2007) PDZ domain binding selectivity is optimized across the mouse proteome. *Science* **317**, 364-369
34. Stiffler, M. A., Grantcharova, V. P., Sevecka, M., and MacBeath, G. (2006) Uncovering quantitative protein interaction networks for mouse PDZ domains using protein microarrays. *J Am Chem Soc* **128**, 5913-5922
35. Tonikian, R., Zhang, Y., Sazinsky, S. L., Currell, B., Yeh, J. H., Reva, B., Held, H. A., Appleton, B. A., Evangelista, M., Wu, Y., Xin, X., Chan, A. C., Seshagiri, S., Lasky, L. A., Sander, C., Boone, C., Bader, G. D., and Sidhu, S. S. (2008) A specificity map for the PDZ domain family. *PLoS Biol* **6**, e239
36. Karlsson, O. A., Sundell, G. N., Andersson, E., Ivarsson, Y., and Jemth, P. (2016) Improved affinity at the cost of decreased specificity: a recurring theme in PDZ-peptide interactions. *Sci Rep* **6**, 34269
37. Thomas, M., Myers, M. P., Massimi, P., Guarnaccia, C., and Banks, L. (2016) Analysis of Multiple HPV E6 PDZ Interactions Defines Type-Specific PDZ Fingerprints That Predict Oncogenic Potential. *PLoS Pathog* **12**, e1005766
38. Luck, K., Charbonnier, S., and Trave, G. (2012) The emerging contribution of sequence context to the specificity of protein interactions mediated by PDZ domains. *FEBS Lett* **586**, 2648-2661
39. Feng, W., Wu, H., Chan, L. N., and Zhang, M. (2008) Par-3-mediated junctional localization of the lipid phosphatase PTEN is required for cell polarity establishment. *J Biol Chem* **283**, 23440-23449
40. Zhang, Y., Appleton, B. A., Wiesmann, C., Lau, T., Costa, M., Hannoush, R. N., and Sidhu, S. S. (2009) Inhibition of Wnt signaling by Dishevelled PDZ peptides. *Nat Chem Biol* **5**, 217-219
41. Cook, D. J., Teves, L., and Tymianski, M. (2012) Treatment of stroke with a PSD-95 inhibitor in the gyrencephalic primate brain. *Nature* **483**, 213-217
42. Cui, H., Hayashi, A., Sun, H. S., Belmares, M. P., Cobey, C., Phan, T., Schweizer, J., Salter, M. W., Wang, Y. T., Tasker, R. A., Garman, D., Rabinowitz, J., Lu, P. S., and Tymianski, M. (2007) PDZ protein interactions underlying NMDA receptor-mediated excitotoxicity and neuroprotection by PSD-95 inhibitors. *J Neurosci* **27**, 9901-9915
43. Nissen, K. B., Haugaard-Kedstrom, L. M., Wilbek, T. S., Nielsen, L. S., Aberg, E., Kristensen, A. S., Bach, A., Jemth, P., and Stromgaard, K. (2015) Targeting protein-protein interactions with trimeric ligands: high affinity inhibitors of the MAGUK protein family. *PLoS One* **10**, e0117668
44. Vitry, S., Ausseil, J., Hocquemiller, M., Bigou, S., Dos Santos Coura, R., and Heard, J. M. (2009) Enhanced degradation of synaptophysin by the proteasome in mucopolysaccharidosis type IIIB. *Mol Cell Neurosci* **41**, 8-18
45. Toli, D., Buttigieg, D., Blanchard, S., Lemonnier, T., Lamotte d'Incamps, B., Bellouze, S., Baillat, G., Bohl, D., and Haase, G. (2015) Modeling amyotrophic lateral sclerosis in pure human iPSc-derived motor neurons isolated by a novel FACS double selection technique. *Neurobiol Dis* **82**, 269-280
46. Maury, Y., Come, J., Piskorowski, R. A., Salah-Mohellibi, N., Chevaleyre, V., Peschanski, M., Martinat, C., and Nedelec, S. (2015) Combinatorial analysis of developmental cues efficiently converts human pluripotent stem cells into multiple neuronal subtypes. *Nat Biotechnol* **33**, 89-96
47. Prehaud, C., Lafon, M., and Schnell, M. J. (2010) Neuron generation, regeneration and protection. *European Patent-PCT* **WO 2010/116258**
48. Zufferey, R., Nagy, D., Mandel, R. J., Naldini, L., and Trono, D. (1997) Multiply attenuated lentiviral vector achieves efficient gene delivery in vivo. *Nat Biotechnol* **15**, 871-875
49. Prehaud, C., Lafon, M., and Lafaye, P. (2015) Nanobodies suitable for neuron regeneration therapy. *WO/2016/038122* **Patent application**

50. Lafaye, P., Achour, I., England, P., Duyckaerts, C., and Rougeon, F. (2009) Single-domain antibodies recognize selectively small oligomeric forms of amyloid beta, prevent Abeta-induced neurotoxicity and inhibit fibril formation. *Mol Immunol* **46**, 695-704
51. Meijering, E., Jacob, M., Sarria, J. C., Steiner, P., Hirling, H., and Unser, M. (2004) Design and validation of a tool for neurite tracing and analysis in fluorescence microscopy images. *Cytometry A* **58**, 167-176
52. Radio, N. M., Breier, J. M., Shafer, T. J., and Mundy, W. R. (2008) Assessment of chemical effects on neurite outgrowth in PC12 cells using high content screening. *Toxicol Sci* **105**, 106-118
53. Yeyeodu, S., Gilyazova, N., Huh, E. Y., Dandepally, S. R., Oldham, C., Williams, A., and Ibeanu, G. (2011) A trifluoromethyl analog of verbenachalcone promotes neurite outgrowth and cell proliferation of NeuroScreen-1 cells. *Cell Mol Neurobiol* **31**, 145-153
54. Sholl, D. A. (1953) Dendritic organization in the neurons of the visual and motor cortices of the cat. *J Anat* **87**, 387-406
55. Lioy, D. T., Garg, S. K., Monaghan, C. E., Raber, J., Foust, K. D., Kaspar, B. K., Hirrlinger, P. G., Kirchhoff, F., Bissonnette, J. M., Ballas, N., and Mandel, G. (2011) A role for glia in the progression of Rett's syndrome. *Nature* **475**, 497-500
56. Chopy, D., Detje, C. N., Lafage, M., Kalinke, U., and Lafon, M. (2011) The type I interferon response bridles rabies virus infection and reduces pathogenicity. *J Neurovirol* **17**, 353-367
57. Prehaud, C., Lay, S., Dietzschold, B., and Lafon, M. (2003) Glycoprotein of nonpathogenic rabies viruses is a key determinant of human cell apoptosis. *J Virol* **77**, 10537-10547
58. Terrien, E., Simenel, C., Prehaud, C., Buc, H., Delepierre, M., Lafon, M., and Wolff, N. (2009) 1H, 13C and 15N resonance assignments of the PDZ of microtubule-associated serine/threonine kinase 205 (MAST205) in complex with the C-terminal motif from the rabies virus glycoprotein. *Biomol NMR Assign* **3**, 45-48

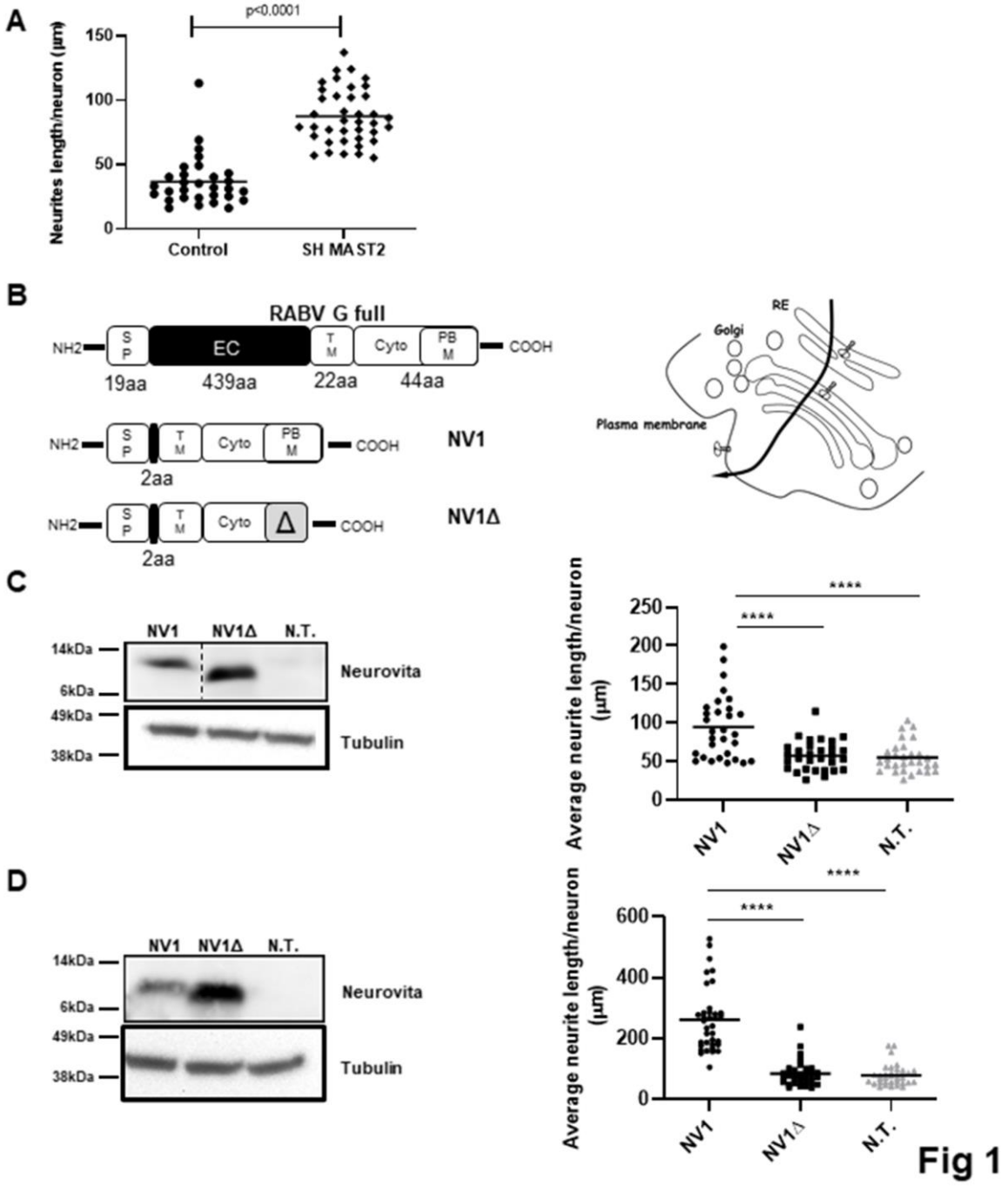


**Figure 1**: **Lentivector-delivered Neurovita 1 (NV1) in SH-SY5Y or NS triggers neurite outgrowth in a PBM dependent manner.**

**A**. Silencing of *MAST2* (SH MAST2) triggers spontaneous neurite outgrowth in SH-SY5Y culture. This effect is not observed when cells were treated with pL.KO1shRNA (Control). Two-tailed unpaired Student's *t*-test, =$p$<0.0001. These results are representative of two independent experiments.

**B**. Structure of the RABV G-protein gene encoding a signal peptide (SP, 19 aa) an extracellular domain (EC), a transmembrane domain (TM, 22 aa) and a cytoplasmic domain Cyto (44 aa) together with a C-terminal PBM. Scheme on the right shows G-protein trafficking from the ER to the plasma membrane in RABV-infected cells. Diagram of the lentiviral vector transgene expression cassettes: NV1 contains

the SP, two amino acids from the EC domain (2 aa), the TM, and the Cyto domain. NV1Δ is identical except that it lacks the last 4 aa at the C-terminus of the PBM.

**C.** Neurite outgrowth triggered by NV1 and NV1Δ in SH-SY5Y cells 24 h post transduction with the lentivectors. Left panel, expression of NV1 and NV1Δ assessed by WB with a RABV G-protein Cyto-specific antibody. The expected MWs of NV1Δ and NV1 are 9.0 and 9.5 kDa, respectively. Expression of tubulin is used as a loading control. To note, NV1 and NV1Δ bands- obtained in the same membrane but on non-contiguous lanes- were spliced (dashed line). Right panel, measurement of neurite outgrowth in SH-SY5Y cells expressing NV1 or NV1Δ 30 h post-transduction. Images of 30 fields (mean of 300 cells per field) were taken with a UV microscope for each condition. The images were analyzed by ImageJ and the NeuronJ plugin to calculate the average neurite length. N.T. = Non-Transduced cells. Results are representative of 6 independent experiments.

**D**. Neurite outgrowth triggered by NV1 and NV1Δ in NS cells 72 h post-transduction with the lentivectors. Left panel, protein levels assessed by WB. Expression of tubulin is used as a loading control. Right panel, measurement of neurite outgrowth in NS cells expressing NV1 or NV1Δ 72 h post-transduction. $N$=36 fields (mean number of cells per field: 324). N.T. = non-transduced cells. Results are representative of 5 independent experiments.

**For C and D**: ANOVA with Bonferroni's multiple comparison post-hoc test, $****=p<0.0001$.

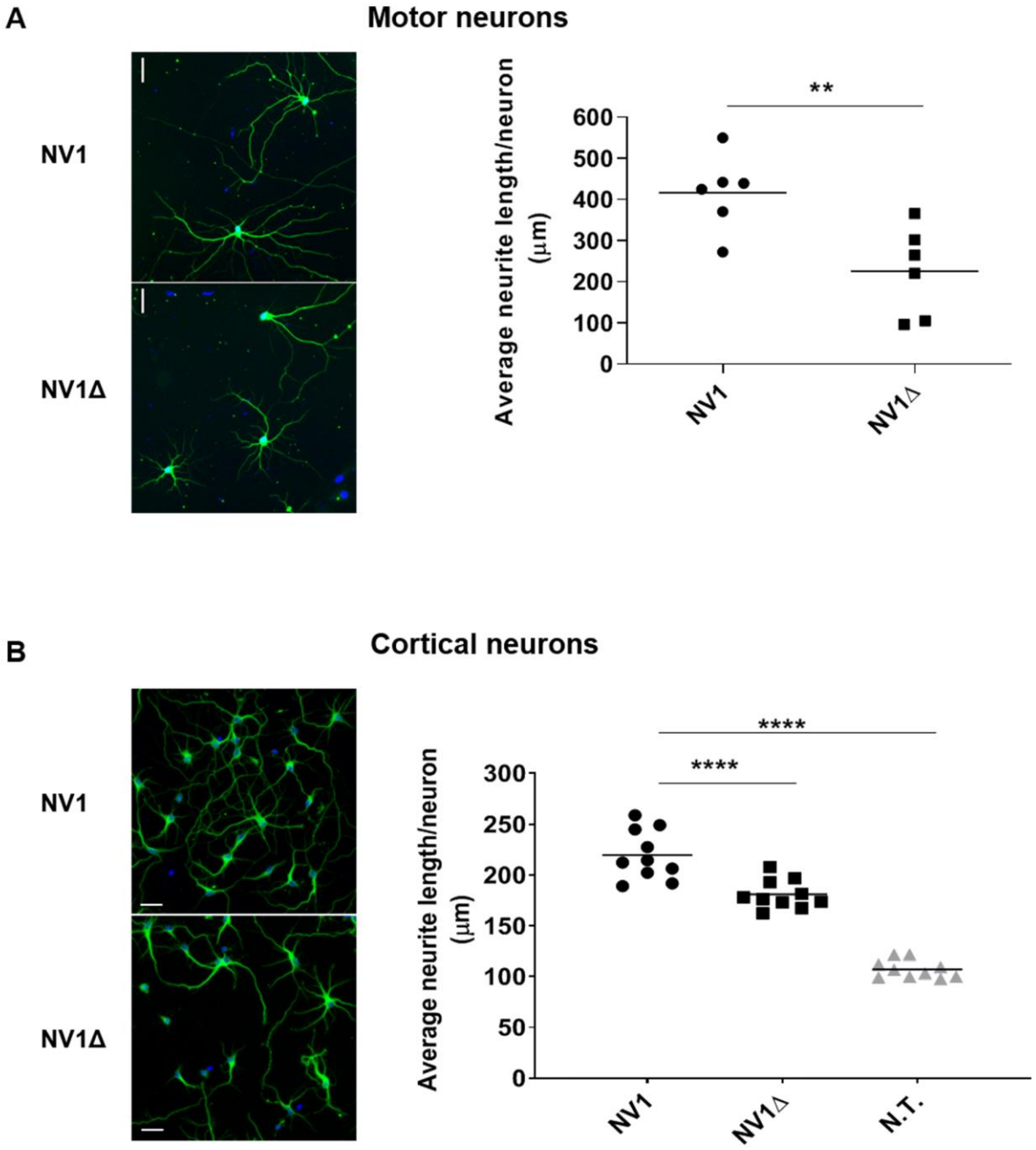


**Figure 2**: **NV1 stimulates neurite outgrowth in human iPSc-derived motor neurons and mouse cortical neurons.**

**A**. Neurite outgrowth in iPSc-derived human motor neurons expressing NV1 and NV1Δ 72 h post-transduction. Images of 6 fields (500 cells) were taken with the Cell Insight Platform. Analysis was performed using the Neuronal Profiling Bio-application. Neurite outgrowth was measured in triplicate wells. Two-tailed unpaired Student's *t*-tests $^{**}$=*p*=0.0081. Scale bar = 20 µm. Results are representative of two independent experiments.

**B**. Neurite outgrowth in mouse cortical neurons expressing NV1 and NV1Δ 72 h post-transduction. Image of 10 fields (mean of 650 cells per field) were taken with the Cell Insight Platform. Neurite outgrowth was measured using the Neuronal Profiling Bio-Application. Neurite outgrowth was measured in triplicate experiments. N.T. = Non-Transduced cells, ANOVA with Bonferroni's multiple

comparison post-hoc test, ****=$p$<0.0001. Scale bar =50 µm. Results are representative of two independent experiments.

**A**

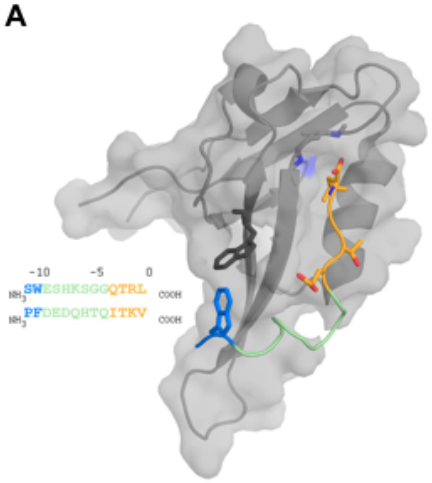


**B**

| PBM | Sequence | $K_D$ (μM) | ΔH (cal/mol) | TΔS (cal/mol) | n |
|---|---|---|---|---|---|
| $_{SW}$Cyto13$_{QTRL}$, **NV1** | SW**ESHKSGG**QTRL | 1.26 ± 0.11 | -9929 ± 143 | -1878 | 1.00 ± 0.02 |
| $_{PF}$PTEN$_{ITKV}$ | PF**DEDQHTQ**ITKV | 1.99 ± 0.05 | -6323 ± 37 | 1452 | 1.19 ± 0.01 |
| 442 | SW**EVHASGG**QTRL | 0.49 ± 0.01 | -10340 ± 64 | -1737 | 1.04 ± 0.01 |
| 443 | SW**AEAQHTQ**QTRL | 0.40 ± 0.01 | -9088 ± 90 | -361 | 1.01 ± 0.01 |
| 439 | SW**EVHTQ**QTRL | 0.21 ± 0.01 | -8454 ± 71 | 647 | 1.02 ± 0.01 |
| 441, **NV2** | SW**EVHGG**QTRL | 0.12 ± 0.01 | -10230 ± 68 | -808 | 1.07 ± 0.01 |
| 453 | SW**EVYTG**QTRL | 0.238 ± 0.003 | -6511 ± 114 | 2521 | 0.85 ± 0.11 |
| 454, **NV3** | SW**EVHGQ**QTRL | 0.0629 ± 0.037 | -8715 ± 204 | 1109 | 1.01 ± 0.01 |
| 455 | SW**EVHTG**QTRL | 0.130 ± 0.024 | -9434 ± 111 | -42 | 0.91 ± 0.07 |
| 460 | SW**EVAGG**QTRL | 0.188 ± 0.027 | -7484 ± 77 | 1687 | 0.92 ± 0.06 |
| 461 | SW**EVATQ**QTRL | 0.126 ± 0.027 | -7688 ± 104 | 1722 | 0.81 ± 0.01 |

**C**

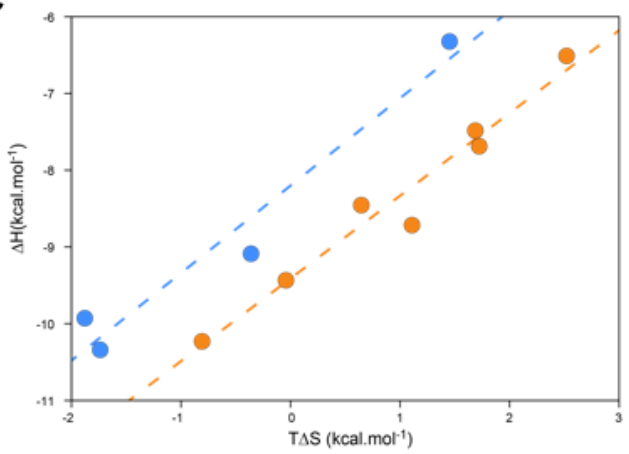


**Figure 3**: **Search for improved NV-PBMs**

**A**. Structure of MAST2-PDZ (in gray) bound to the viral peptide Cyto13 (PDB code 2KQL). The N-terminal anchor, the linker, and the C-terminal anchor of Cyto13 are shown in blue, green and orange, respectively. The 13 C-terminal aa of NV1 and PTEN are indicated.

**B.** Thermodynamic parameters from ITC experiments for 11 peptides interacting with MAST2-PDZ.

**C.** Enthalpy (ΔH) and entropy (TΔS) values for peptides from the first and second rounds of optimization are shown in blue and orange, respectively. Values for NV1, 2 and 3, and PTEN peptides are indicated.

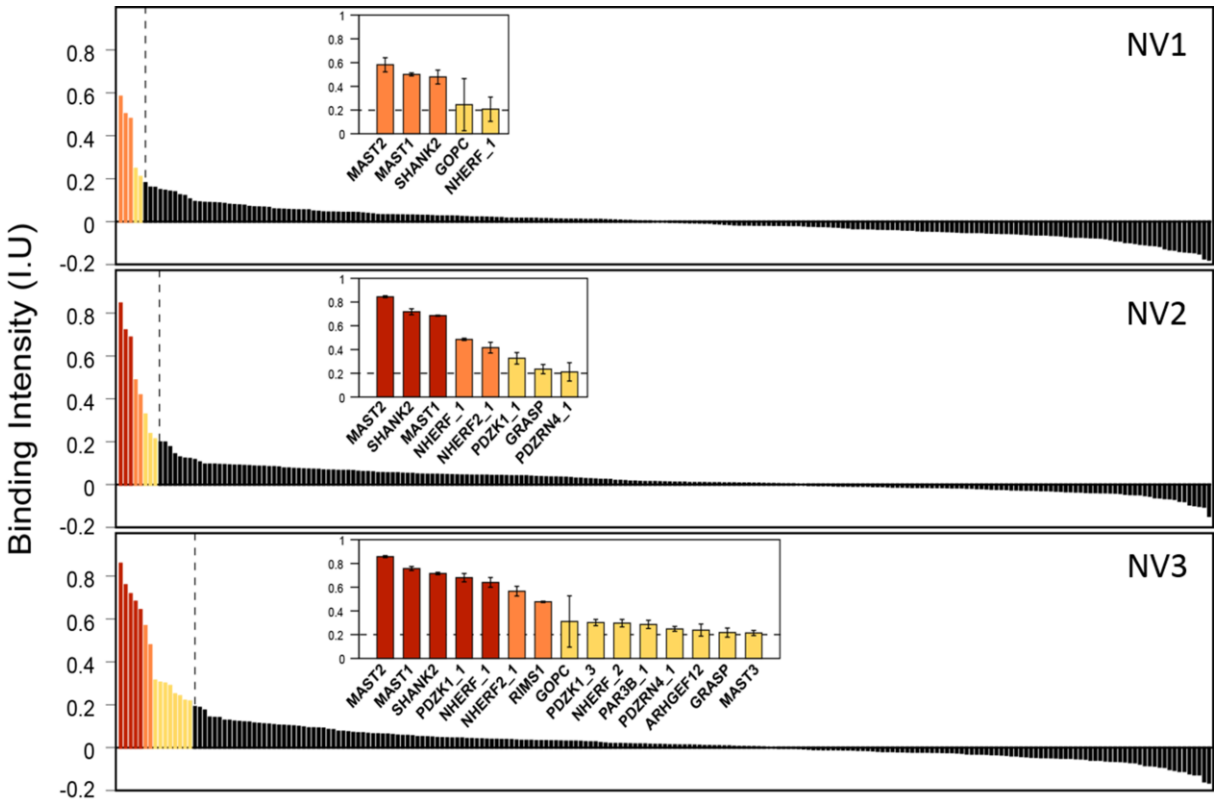


**Figure 4**. **PDZome binding profiles for NV peptides**. PDZ domains (*x* axis) are ranked in descending order of binding intensity (BI) (y axis). Magnifications showing the best binders of NV1, 2 and 3 (BI > 0.2 IU). BI values greater than 0.6 IU, between 0.3 IU and 0.6 IU, and lower than 0.3 IU are shown in red, orange and yellow, respectively. Biotin was used as a control for the BI profile.

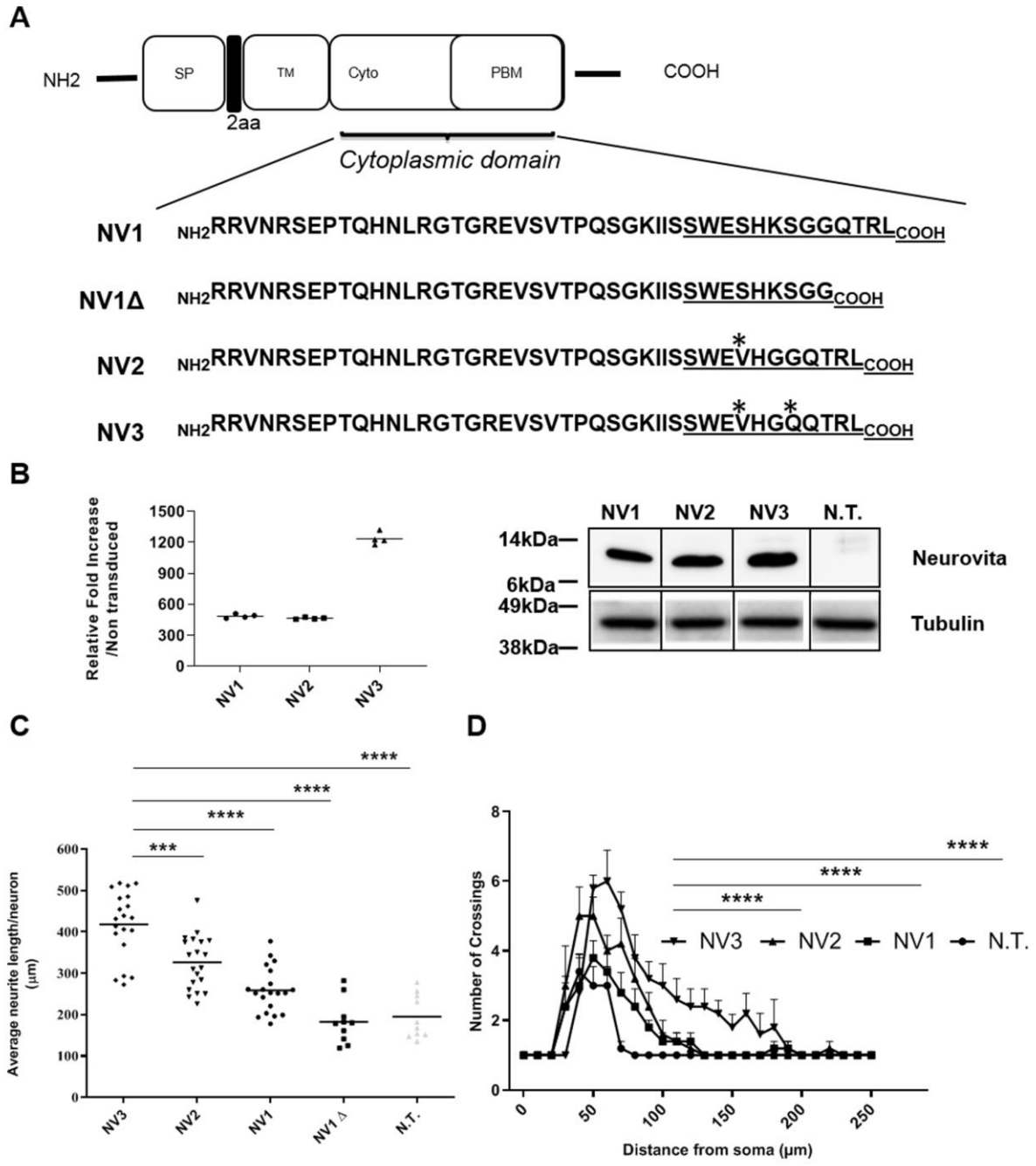


**Figure 5**: **Increasing the affinity of NV-PBMs for MAST2 protein increases their biological activity**

**A**. Diagram of the lentiviral transgene expression cassettes showing the length of the cytoplasmic domain of the constructs (44 aa for the Cyto domain of NV1 and 42 aa for the Cyto domains of NV2 and NV3). The PBM is underlined. Star * indicates the replacement or the deletion of one residue.

**B**. Transduction efficiencies for NV1, NV2 and NV3, as assessed by RT-PCR (left) or by WB on NS cells 48 h post-transduction with lentivectors. NT= Non-Transduced cells. Tubulin was used as a loading control.

**C**. Neurite outgrowth of NV3-, NV2-, NV1-, and NV1Δ-expressing NS cells 72 h post-transduction. *N*=20 fields (NV3, NV2, NV1), =10 fields (NV1Δ, N.T.). ANOVA with Bonferroni's multiple comparison post-hoc test, ***=p=0.0002, ****=$p$<0.0001. Results are representative of three independent experiments.

**D**: Arborization (Sholl analysis) in NV3-, NV2- and NV1-expressing NS cells 72 h post-transduction. The analysis was performed in the same sets of NV1-, NV2- and NV3-treated NS cells. *N*=10 fields (NV3, NV2, NV1, NT) Two-way ANOVA $^{****}p<0.0008$. Results are representative of three independent experiments.

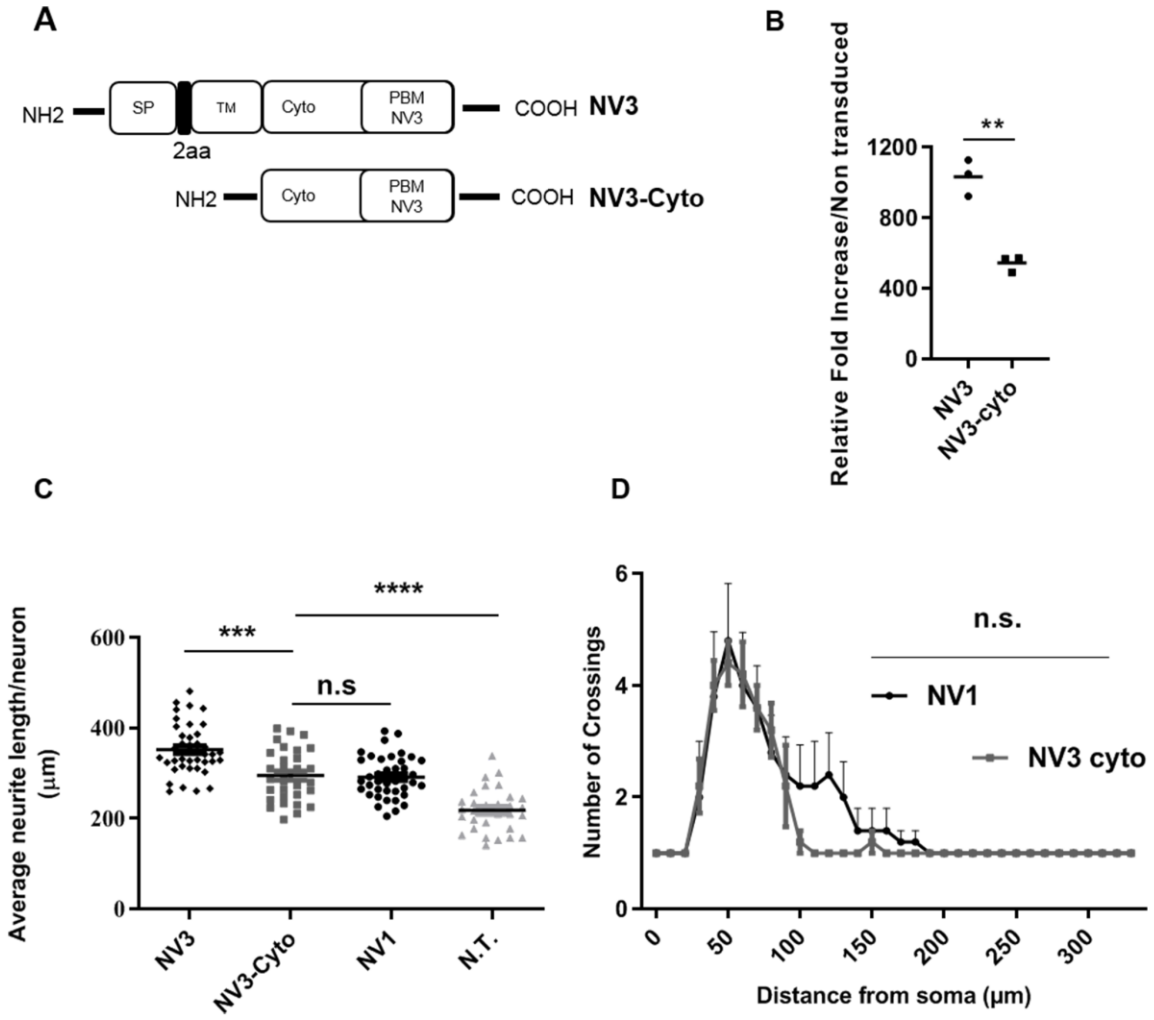


**Figure 6**: **NV3-Cyto is as efficient as NV1**

**A**. Diagram of the two NV3 lentivector transgene constructs. NV3-Cyto is truncated and lacks the SP, the 2 aa from the EC domain, and the TM domain. It consists of the Cyto domain of NV3 only.

**B**. Transcription of the NV3, NV3-Cyto and NV1 transgenes in NS cells. 18S is used as the standard. *N*=3. Two-tailed unpaired Student's *t* tests, **=*p*=0.0017.

**C**. Neurite outgrowth in NV3-, NV3-Cyto- and NV1-expressing NS cells 72 h post-transduction. NT =non-transduced cells. *N*=30 fields (NT, NV3-cyto), *N*=40 fields (NV1, NV2, NV3). ANOVA with Bonferroni's multiple comparison post-hoc test. Two-tailed unpaired Student's *t*-tests, ***=*p*=0.0002, ****=*p*<0.0001. Results are representative of three independent experiments.

**D** Arborization (Sholl analysis) for NV1- and NV3-Cyto-expressing NS cells 72 h post-transduction. NT = non-transduced cells. *N*=5 fields, two-way ANOVA. n.s= not significant. Results are representative of three independent experiments.

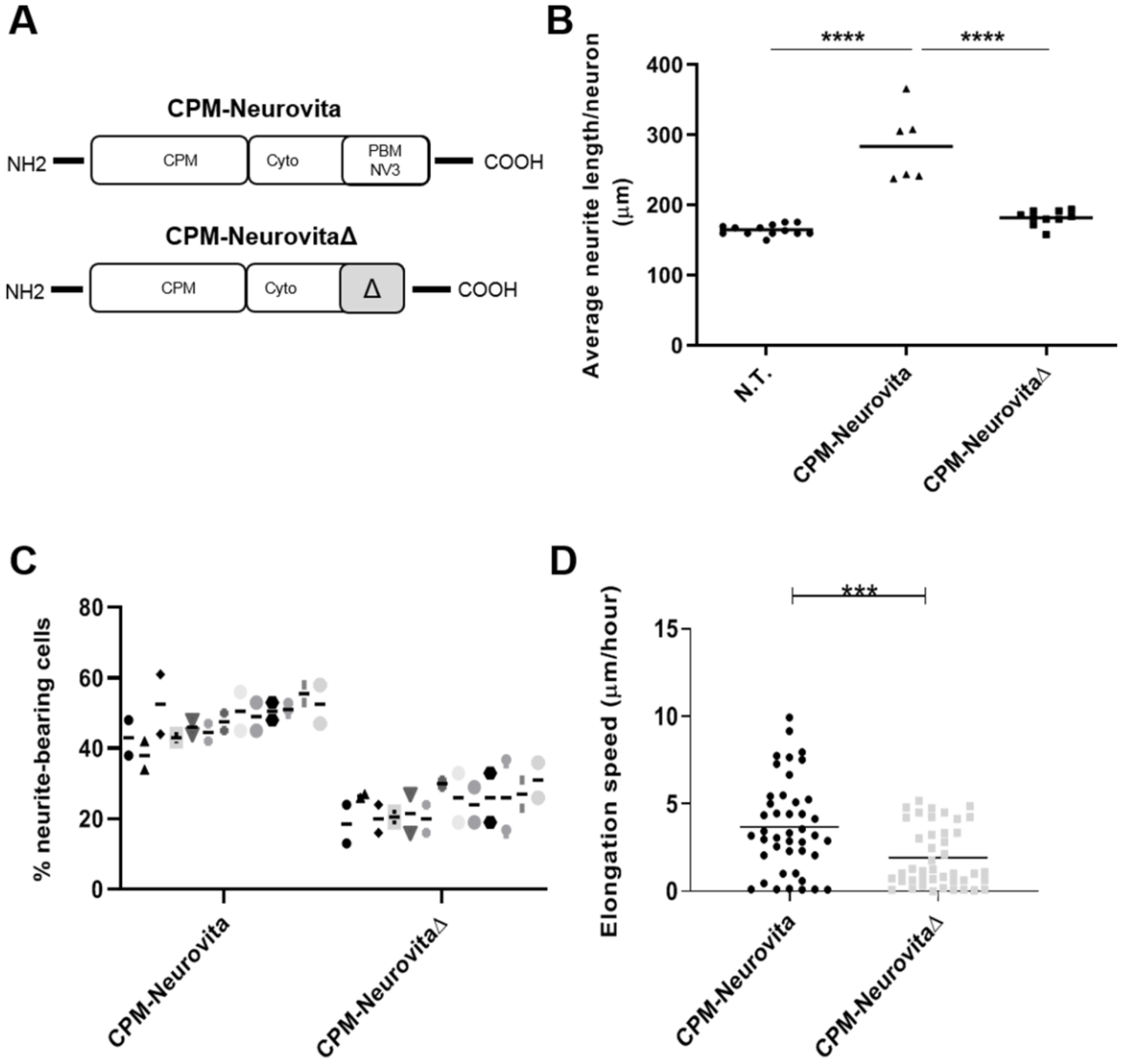


**Figure 7. Delivery of Neurovita as a peptide using a CPM.**

**A.** Diagram of the CPM-Neurovita molecule and its PBM-deleted counterpart (CPM-NeurovitaΔ). CPM=Cell-Penetrating Molecule.

**B.** Neurite outgrowth in CPM-Neurovita/CPM-NeurovitaΔ- transduced or non-transduced (NT) NS cells 72 h post treatment. *N*=13 fields (NT), *N*=6 fields (CPM-Neurovita), *N*=10 fields (CPM-NeurovitaΔ). Two-tailed unpaired Student's *t*-test, ****=$p<0.0001$. Results are representative of four independent experiments.

**C.** NS neurite outgrowth was monitored by live-cell imaging on Incucyte (Sartorius, USA) in nine fields ((mean of 43 cells per field) and analyzed with ImageJ and NeuronJ plugin. Percentage of neurite-bearing NS cells (53) after treatment with either CPM-Neurovita or CPM-NeurovitaΔ. Over a 12 h time

period, from 18 h to 30 h post treatment, CPM-Neurovita triggered neurite outgrowth in NS cells in a PDZ-BM-dependent manner. The marks correspond to the percentages of neurite bearing cells observed every hour over the 12 hours period in CPM-Neurovita treated culture (left) or in CPM-NeurovitaΔ treated culture (right). Two-way ANOVA, $p<0.0001$. Results are representative of two independent experiments.

**D:** Over this 12-hour period, the speed of outgrowth, expressed as µm/hour, was monitored on the recorded live cell images. CPM-Neurovita increased the speed of neurite outgrowth in the NGF-treated NS cells. Two-tailed unpaired Student's *t*-tests, $p=0.0005$. Results are representative of two independent experiments.

**Supporting Information :** Structure-based optimization of a PDZ binding motif within a viral peptide stimulates neurite outgrowth. Khan Z. et al, revision July 2019

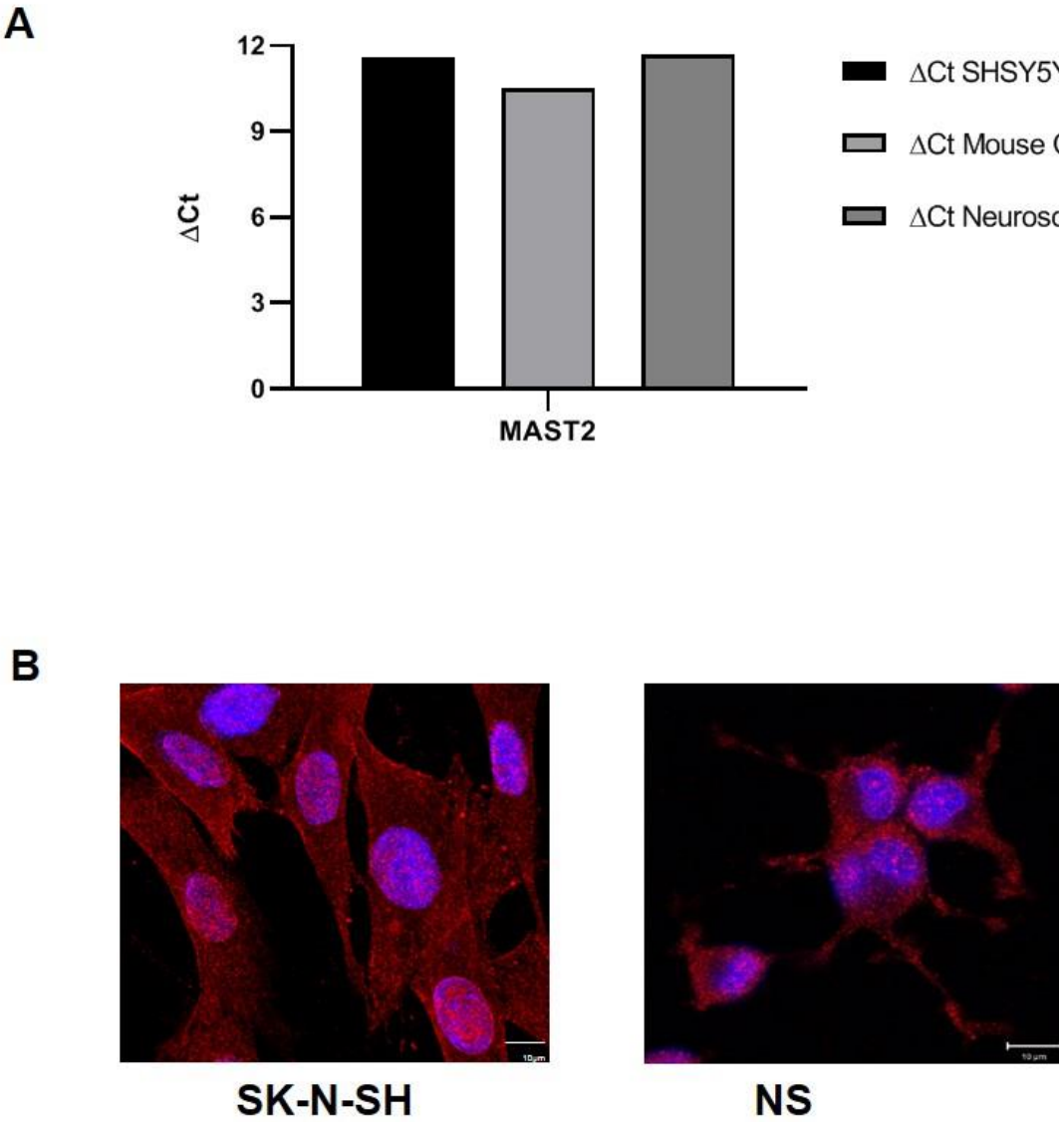

**Figure S1. Relevance of the *in vitro* biological models**

**A**. Detection of MAST2mRNA by Q-PCR. The ΔCt is the Ct obtained for MAST2 minus the Ct of the reference gene (18S). In these conditions the transcripts of a gene is considered non-detected for a ΔCt>22.

**B.** Immunofluorescence detection of MAST2 protein in neuronal cells, SK-N-SH (left) and NS cells (right). MAST2 is in red, nuclei are in blue. Bars are 10µm. Two-tailed unpaired Student's *t*-test, =$p$<0.0001. These results are representative of two independent experiments.

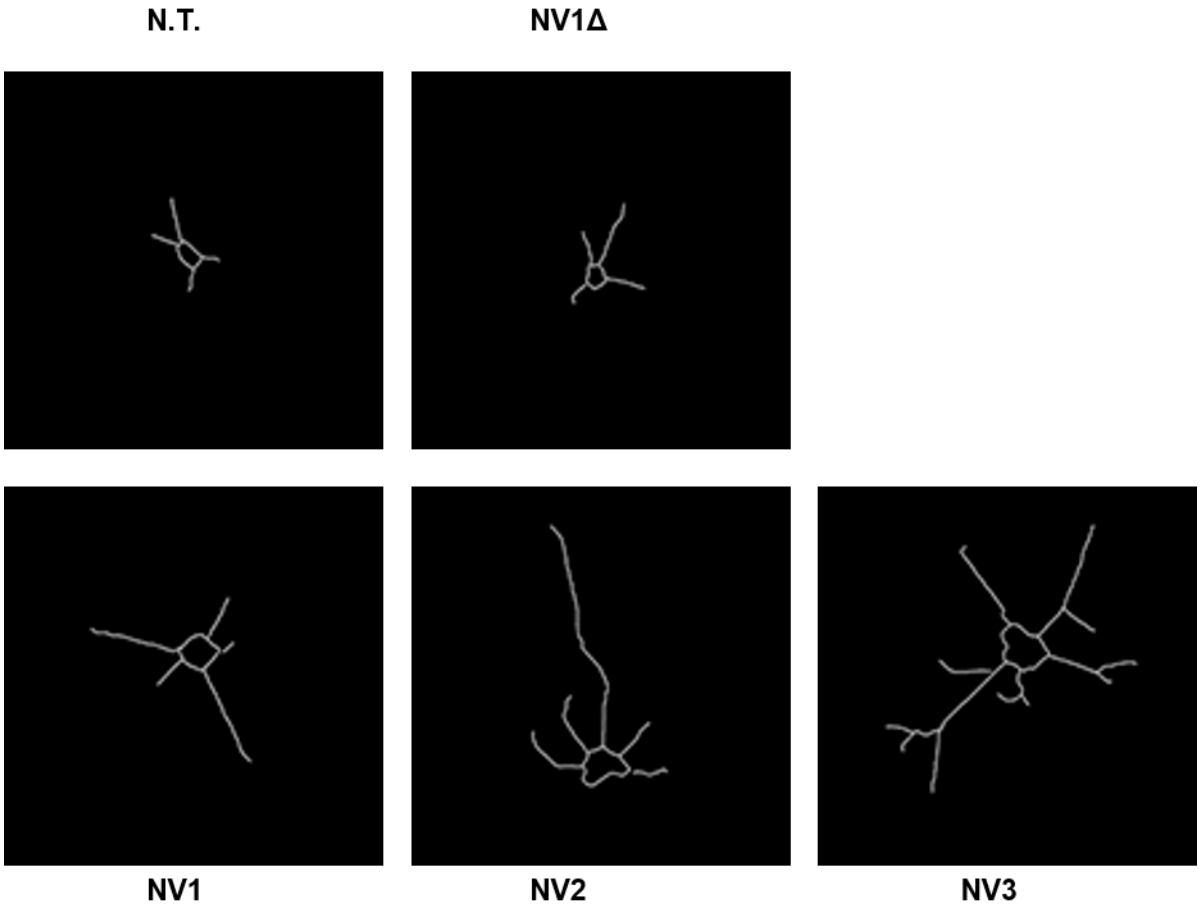


**Figure S2. Representative NeuronJ tracing of the NS cells phenotypes following lentivectors delivery of NV molecules.**

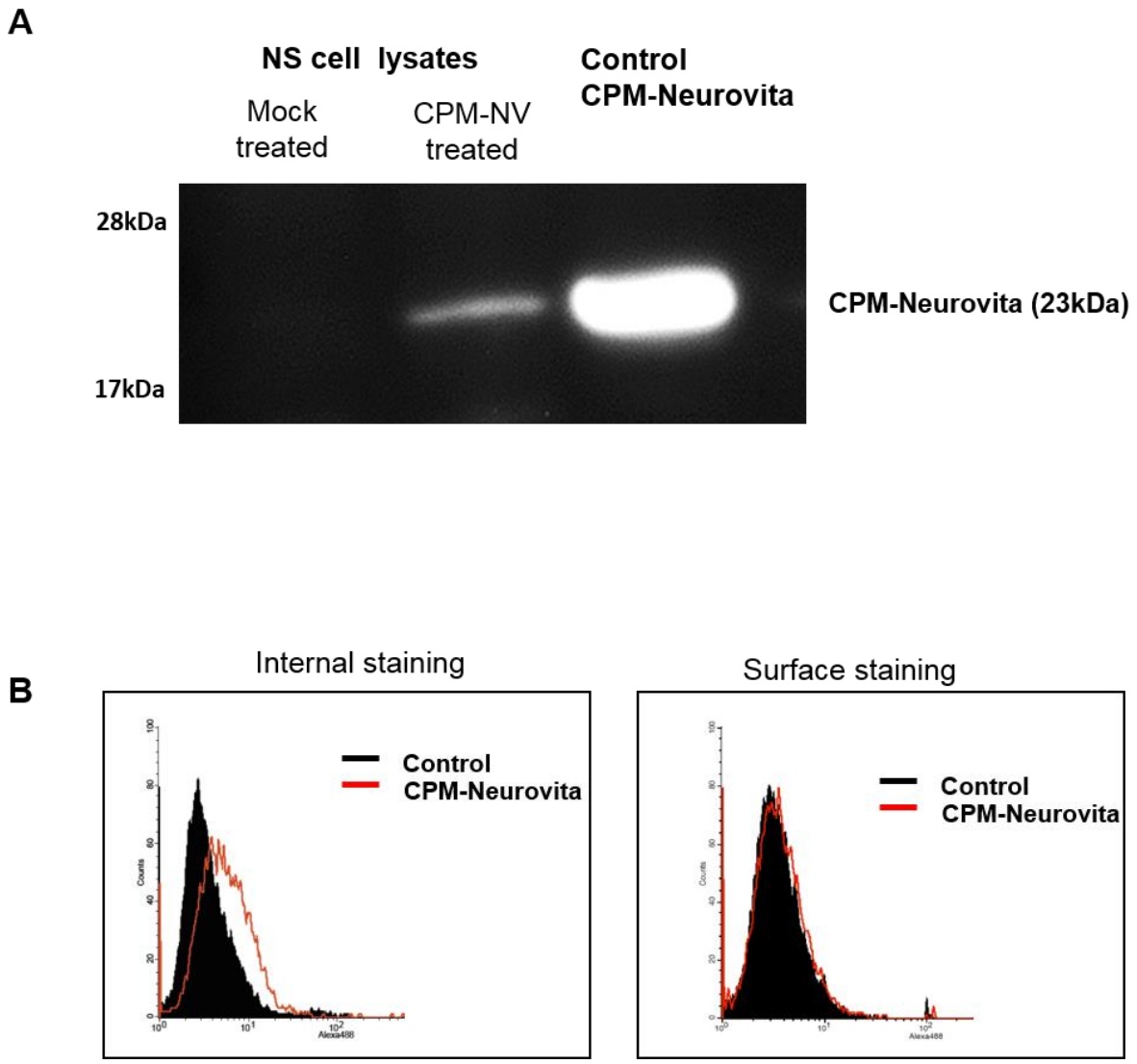


**Figure S3. CPM-Neurovita associates with cells when added to the culture medium**

**A.** Western blotting detection of CPM-Neurovita in NS cells 6 hours after treatment with the CPM-Neurovita (CPM-NV) or mock-treated. The control CPM-Neurovita is a loading control. These results are representative of two independent experiments.

**B**. Flow cytometry detection of CPM-Neurovita after 30mn treatment (4°C) of NGF differentiated NS cells. The internal staining is shown on the left, the surface staining on the right. Black histogram represents the control condition. The cells treated with CPM-Neurovita correspond to the red solid line. These results are representative of two independent experiments.